THESIS TITLE

by

Kara Kundert

A thesis submitted in partial satisfaction of the

requirements for the degree of

Master of Astrophysics

in

Astronomy

in the

Graduate Division

of the

University of California, Berkeley

Committee in charge:

Professor Aaron Parsons, Chair
Professor Martin White
Professor Eugene Chiang

Fall 2018

The thesis of Kara Kundert, titled THESIS TITLE, is approved:

Chair _____ Date _____

_____ Date _____

_____ Date _____

University of California, Berkeley

THESIS TITLE

Copyright 2018
by
Kara Kundert

Abstract

THESIS TITLE

by

Kara Kundert

Master of Astrophysics in Astronomy

University of California, Berkeley

Professor Aaron Parsons, Chair

We seek to lay out the case for the viability of a monopole interferometer to search for the "global signal" of reionization. We believe this is best understood through the Fourier context of spatial modes, where we can push the low-mode monopole into higher-order modes via spatial windowing. This windowing is managed through the use of absorptive walls around the antennas of the array, which modify each antenna's receptivity of the sky, thus introducing spatial variation into the monopole signal. We can characterize the parameters of these walls and their effects on our observed signal into a set of known sensitivity coefficients, which can then be used to accurately recover the reionization global signal. From our exploration of these parameters, we are able to now state with certainty that we are able to detect the monopole term of the sky using a classical interferometer, and would recommend further investigation into the subject for those seeking to observe and better understand the early history of the Universe.

Failure is simply the opportunity to begin again,
this time more intelligently.
– Henry Ford

Contents

Contents **ii**

List of Figures **iii**

1 The Global Signal – Its Physics and Significance to Cosmology **1**
1.1 Overview of the Epoch of Reionization 1
1.2 Overview of the Global Signal 3

2 Interferometry **6**
2.1 Brief Overview 6
2.2 Spatial Modes and Interferometric Sensitivities 9
2.3 Observing the Spatial Monopole with an Interferometer 12

3 Overview of the Theory of HYPERION **15**
3.1 Absorber – A New Approach to Monopole Interferometry 15
3.2 Overview of the Instrumental Design 19

4 Overview of the Logistics of HYPERION **20**
4.1 Methodology of Simulation 20

5 Sensitivity to the Monopole Sky **27**
5.1 Simulated Visibilities 27
5.2 Recovered Global Signal 32

6 Conclusion **39**

A The Flat-Sky Approximation and Its Limitations **41**

Bibliography **42**

List of Figures

1.1 In the top half of the figure, we see a cartoon of the reionization history of the universe and the development and growth of ionized bubbles over time. In the bottom half, we see a breakdown of T_b, the brightness temperature of the 21 cm global signal, over time. There are five labeled regimes to this plot, each corresponding to the dominance of a different variable in the production of the 21 cm signal. Figure originally published in Pritchard & Loeb 2012. 4

2.1 Above, we see a collection of the low-order spherical harmonic functions. This can help us begin to visualize what, physically, the spherical harmonics are and how they can be used to parse spatial information observed on the sky from an interferometer. 11

2.2 This figure shows the Fourier relationship between the two-dimensional top hat function and a Bessel function. This image can be thought of as an idealized cartoon of the aperture and visibility planes of our proposed interferometer. On the left, we see the imposed top-hat, where the yellow portion would be the portion of monopole sky visible to the antenna and the blue would be the perfect absorber. On the right, we have performed a two-dimensional Fourier transform to convert into the visibility plane (i.e. to see the spatial modes to which we are observationally sensitive), and we see this rippling function centered around the zero-spacing mode. WRITE DOWN MATHEMATICAL RELATIONSHIP AS WELL 13

3.1 This cartoon shows the basic structure of the proposed absorber walls. Each antenna in the array will be circled by a cylinder of absorber material, creating a uniform temperature cutoff in the antenna's reception of the sky. By increasing the height of the wall, we can change the cutoff angle of the reception of the sky, thereby shrinking the spatial windowing and pushing more of the monopole to higher spatial modes. 18

4.1 Here we see the results of a closed-box return loss measurement taken with a densely packed (i.e. 9×9 tiles per wall) configuration of ferrite tiles, evenly spaced along the walls of the testing Faraday cage. The ripples are an artifact from the testing setup, and not inherent to the performance of the ferrite itself. As can be easily seen, the Ferrite performs much better at the high range of our science band, and is optimized around 120 MHz. While this material has the best performance out of all the materials we have looked into so far, we would ideally prefer a material with a more even absorptivity across the band, so as best to avoid inadvertently adding ripples or structure to our sky observations. 22

4.2 Shown here is a simple diagnostic field set-up that could be used to evaluate an absorber's ability to mitigate cross-talk between elements. Here we used a densely-packed configuration of ferrite tiles that have been propped up on some of our pyramidal foam absorber for additional height. 24

5.1 Shown here is the absolute value of the visibility of a spectrally flat monopole sky versus frequency. In this case, there are no absorptive baffles, just the terrestrial horizon. As can be seen already, the interferometer does have non-zero sensitivity to the monopole, though it is plainly clear that the autocorrelation term (shown in blue) is more sensitive than any of the non-zero interferometric baseline pairings. 28

5.2 Shown here is the absolute value of the visibility of a spectrally flat monopole sky with no absorber walls versus uv-baseline. As can be seen already, the interferometer has a non-zero sensitivity to the monopole at non-zero baseline separations. 29

5.3 Shown here is the absolute value of the visibility of a spectrally flat monopole sky versus frequency, for an array with absorptive baffles constructed from ferrite tiles. In comparison to Fig. 5.1, we see that the reception of the monopole signal has increased at higher frequencies. This indicates that imposing the top-hat windowing function has indeed had the intended effect of pushing the monopole sky into higher-order spatial modes, increasing our array's sensitivity to the global signal. 31

5.4 Shown here is the absolute value of the visibility of a spectrally flat monopole sky with ferrite absorber walls versus uv-baseline. We can see that, in comparison to Fig. 5.2, the overall shape of the characteristic monopole sensitivity is stretched in uv-space, indicating that our imposed top-hat windowing function has had the intended effect of pushing the monopole into higher order (and more sensitive) spatial modes. However, we also see that the sensitivity of the various baseline pairings of the array no longer fall on top of one another. This is due to the frequency-dependent nature of the ferrite as an absorber. Were we to find a way to even out the absorptivity of the baffles in frequency, we would see that the monopole sensitivities would also even out relative to each other, and we would be better able to take advantage of the overlapping samples in uv-space. 33

5.5 Shown here is the recovered reionization global sky temperature, as measured from a maximally redundant seven element east-west array with a total integrated observation time of five hours, a flat system temperature of $T_{sys} = 300$ K, and pure ferrite absorber baffles. As can be seen, this method of observing the global sky temperature works well, with nearly perfect recovery of the true monopole sky at low frequencies (where our array has the highest sensitivities to the monopole mode) and only small fluctuations (on the order of 3 mK) being introduced at the low-sensitivity high-frequency end of our science band. Although this is a highly idealized case, this is a positive result, indicating that our method of weighting observations can accurately recreate the true 21cm reionization global signal. . 35

5.6 Shown here is the absolute value of the visibility of a spectrally flat monopole sky versus frequency, for an array with absorptive baffles constructed from a material with a flat absorptivity of 15 dB across the science band. Overall, this case that the lowest absolute sensitivity to the monopole across the band, but it also has the flattest slope for the drop-off in sensitivity, meaning the whole band has relatively higher sensitivity if an observation is integrated just a little while longer. 36

5.7 Shown here is the recovered reionization global sky temperature, as measured from a maximally redundant seven element east-west array with a total integrated observation time of five hours and a flat system temperature of $T_{sys} = 300$ K. In this case, the data was collected from an array using ferrite absorber baffles, but was calibrated assuming the absorber baffles had a flat absorptivity of 15 dB across the science band. As can be seen, even with this intentional gross miscalibration of the system, we are still able to recreate a fairly accurate portrayal of the true 21cm reionization global signal, with the only major difference being a slight 5 mK exaggeration of the depth of the absorption feature. This indicates that our weighting method is robust to an imperfect calibration of the performance of the absorptive baffles – a promising result for the feasibility of the project. 38

Acknowledgments

These are the acknowledgements.

Chapter 1

The Global Signal – Its Physics and Significance to Cosmology

1.1 Overview of the Epoch of Reionization

In brief, the Epoch of Reionization refers to the period of the universe's history during which its supply of intergalactic hydrogen became reionized. This is important to its evolution, and therefore of interest to astronomers, due to the driving factor of that ionization: the ignition of the first stars, galaxies, and black holes in the universe. A positive detection of the Epoch of Reionization will help astronomers to clarify many open questions of cosmology, such as the properties of the first galaxies, how stars with zero metallicity formed, the physics of early quasars, and more.

In slightly more detail, let us begin at the beginning. At the start of time, the universe was extremely hot and ionized from the Big Bang. Over time, as space itself expanded and the gas within the universe cooled adiabatically at a rate of $T(z) = (1+z)T_0$, the temperature of the universe dropped low enough that the nearly-uniform ionized plasma that made up the universe was able to recombine to form neutral hydrogen. This phase transition, which occurred approximately 380,000 years after the Big Bang at a redshift of $z = 1098$, enabled photons to decouple from the baryonic matter, thus allowing photons to stream freely for the first time in the history of the universe. These important periods of the universe's history are aptly referred to as "photon decoupling" and "the surface of last scattering". The surface of last scattering also marks the horizon of the observable universe, as everything beyond it is simply too opaque to be observable. The radiation released at the surface of last scattering, now referred to as the "Cosmic Microwave Background" (CMB), has a mean temperature of $T_0 = 2.725$ K (Fixsen 2009) and was first observed serendipitously by Arno Penzias and Robert Wilson in 1964 (Penzias & Wilson 1965).

At the point of the CMB, the gravitational force had heretofore always served as second fiddle to the electromagnetic force, and the formation of structure was driven solely by dark matter (Zaroubi 2012). As such, structure had yet to form, and the release of the CMB

led to a period known as the "Dark Ages" – a time when the universe had nothing to do but slowly get to work allowing slight matter over-densities, i.e. approximately 1 part in 10^5 more dense than the mean density of the universe according to COBE observations (Wright 1992), to grow and transform into stars, galaxies, and black holes.

About 100 million years passed and the universe bathed in nothing but the after-glow of the Big Bang. Finally, the first galaxies formed, and along with them bright stars to emit ionizing radiation. Soon, we find small ionized bubbles in the intergalactic medium (IGM), the hydrogen gas filling the space between galaxies. Over time, more galaxies and their bright stars make more ionized bubbles, until eventually the entire universe's supply of loose hydrogen gas has been converted into a proton-electron ionized plasma.

This period, very creatively, is called the Epoch of Reionization – the epoch during which the universe once again became ionized, like it was at the dawn of time. As of yet, there has been no confirmed direct detection of the physics of this time period – either of the objects that drive it nor of the gas behavior itself. This has not been for lack of trying.

For example, EDGES is a small ground-based antenna system in the Murchison Radio-astronomy Observatory in Western Australia seeking to detect the 21cm reionization global signal directly. It features two broadband single polarization dipole-like blade antennas, one low-band (50-100 MHz) and one high-band (90-190 MHz), with a 30x30 m metal ground screen below (Monsalve et al. 2017). While there has yet to be a confirmed direct detection of the Epoch of Reionization, the EDGES experiment has announced a possible detection of the 21 cm reionization global signal (Bowman et al. 2018).

SARAS, similarly, is a 21cm reionization global experiment based in India, using a frequency independent fat dipole antenna and a correlation spectrometer to measure the average sky temperature across the octave band 87.5-175 MHz (Patra et al. 2013). Unlike EDGES, SARAS implements an absorptive ground screen rather than a reflective one.

Another tactic to reionization studies is to look for the power spectrum signature, rather than the global average phenomena. This is the path taken by the PAPER and HERA experiments, both located in the Karoo Desert of South Africa and headquartered here in Berkeley, California (DeBoer 2017). While the power spectrum signal is expected to be fainter than that of the global signal, it is also better suited to be observed with a traditional interferometer, which relieves some of the fine-tuned calibration concerns that plague global signal studies.

There are many others as well, in all states of existence – SCI-HI (now PRI^{Z}M) with its distinctive HIbiscus antenna design (Voytek et al. 2014), LOFAR attempting to use its general purpose instrument in a very specialized way (Rottgering 2006), DARE proposing to take the search for cosmic reionization in space itself (Burns 2012), and more. As it turns out, these observations are hard to make – 13 billion light years is a long way for light to travel. And that's not even accounting for the blinding synchrotron emission from our own galaxy getting in the way, washing out the reionization signals at a scale of 100,000 to 1.

For the sake of brevity and intellectual focus, this thesis (and the experiment proposed within) will be focusing solely on observing the overall average behavior of the intergalactic medium as it evolves throughout this time period. This is referred to as the "global signal".

1.2 Overview of the Global Signal

The global signal of reionization is an observation of the overall average nature of hydrogen throughout this epoch, i.e. the spatially averaged signal from the neutral hydrogen gas, as observed using redshifted 21 cm emission from the intergalactic medium 13 billion years ago. More specifically, global signal experiments seek to observe the relationship between the internal level populations of the neutral hydrogen IGM and the ambient temperature of the universe, as set by the CMB photons. This relationship is written quantitatively in Eq. (1.1).

$$\delta T_b = (T_s - T_\gamma)(1 - e^{-\tau}) \tag{1.1}$$

where δT_b is the observed fluctuation in the 21 cm brightness temperature of the 21 cm line (T_s) relative to the background CMB brightness temperature (T_γ), and τ is the optical depth of the hydrogen through which the CMB is passing.

By observing the evolution of the spin temperature relative to the CMB background temperature, we are able to better understand how and when energy was injected into the gas (Pritchard & Loeb 2010). For example, the X-rays generated by black holes contributed to the heating of the gas, making the gas itself brighter than the ambient photons. Additionally, Lyman-α photons from Population II and III stars modify the coupling of the IGM gas temperature to the 21 cm spin temperature via the Wouthuysen-Field effect, providing a means to track early star formation (Furlanetto et al. 2006).

However, while it's fairly straightforward to observe the 21 cm signal and acquire a measurement of the spin temperature through time, that alone doesn't give us much insight into the driving physics of that signal. First, we must understand what factors contribute to the spin temperature of the gas.

Brief History of the Global Signal

The most important observable quantity of the global signal, and the one that informs us as to the underlying astrophysics at each redshift, is the spin temperature T_s, which can be described as a weighted average of of the ambient CMB photon temperature T_γ, the kinetic temperature of the intergalactic medium T_K, the collisional excitation ratio x_c, and the Lyman-α excitation ratio x_α, as shown in Eq. (1.2).

$$T_s^{-1} = \frac{T_\gamma^{-1} + (x_c + x_\alpha)T_K^{-1}}{1 + x_c + x_\alpha} \tag{1.2}$$

The collisional and Lyman-α excitation ratios define the fraction of transitions that are being driven by ambient CMB radiation vs. by other physical processes (such as collisions or absorption of high energy Lyman-α photons),

$$x_n = \frac{N_{10}}{A_{10}} \frac{T_*}{T_\gamma} \tag{1.3}$$

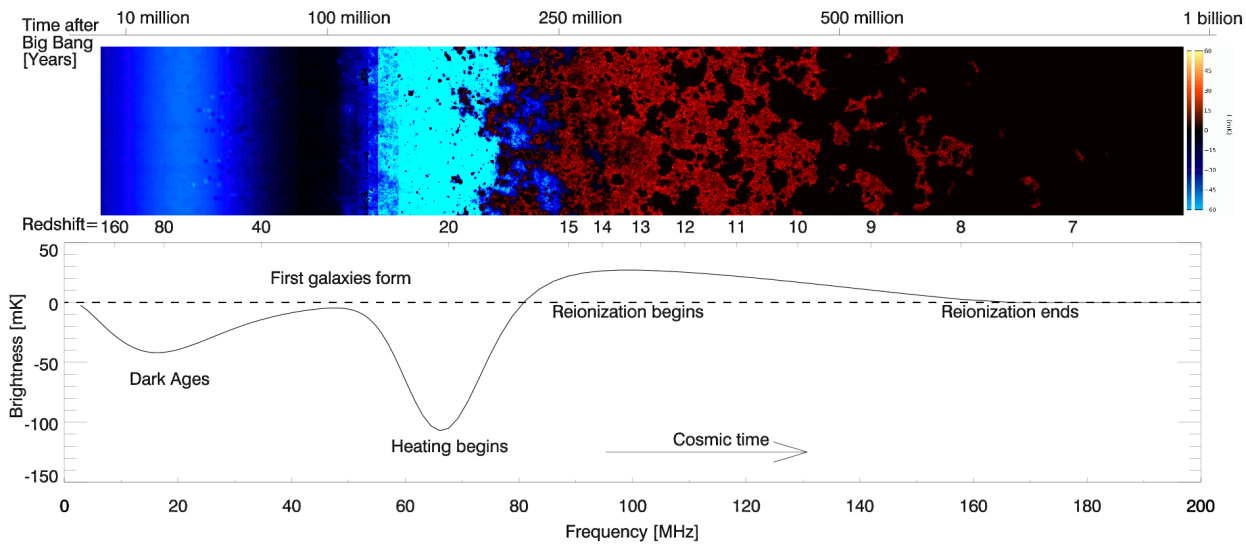

Figure 1.1: In the top half of the figure, we see a cartoon of the reionization history of the universe and the development and growth of ionized bubbles over time. In the bottom half, we see a breakdown of T_b, the brightness temperature of the 21 cm global signal, over time. There are five labeled regimes to this plot, each corresponding to the dominance of a different variable in the production of the 21 cm signal. Figure originally published in Pritchard & Loeb 2012.

where here N_{10} is the excitation rate coefficient of the physical process in question (i.e. the rate at which that particular physical process is driving transitions).

Based on these variables, we can define six main physical regimes believed to have taken place during the process of structure formation and IGM reionization, which can be seen in Fig. 1.1 and are physically detailed below.

- $(200 \leq z \leq 1100)$: During this time period, the residual free electron fraction remaining post-recombination and the high gas density allows the thermal and spin temperatures of the gas to remain coupled with the photon background via Compton scatting and collisional excitations. All temperatures are the same, and therefore there will be no detectable 21 cm signal.

- $(40 \leq z \leq 200)$: As cosmological expansion continues, Compton scattering no longer couples the thermal temperature of the gas to the CMB photons, and the gas and radiation decouple and go out of equilibrium. Collisional coupling sets the spin temperature $T_S < T_\gamma$, leading to an absorption feature in the 21 cm global signal.

- $(30 \leq z \leq 40)$: Expansion continues and collisional interactions are no longer effective at coupling the thermal and spin temperatures of the gas. The excitation levels shift

to being set by radiative coupling to the CMB, such that $T_S = T_\gamma$, and there is no detectable 21 cm signal.

- ($15 \leq z \leq 30$): As the first sources (e.g. stars, active galactic nuclei (AGN), etc...) ignite, they begin emitting high energy Lyman-α and X-ray photons. The hyperfine populations couple to the thermal temperature of the cold gas via the Wouthuysen-Field effect, such that $T_S \sim T_K < T_\gamma$, resulting in an absorption feature in the 21 cm global signal.

- ($7 \leq z \leq 15$): The radiation (particularly the X-rays) from bright sources heat the gas, $T_K > T_\gamma$ and we see 21 cm emission in the global signal. Lyman-α coupling is still effective at setting the level populations.

- ($z \leq 7$): Enough ionizing radiation has spread throughout the universe that the IGM has been converted from neutral to ionized, and reionization is complete.

At present, all redshift ranges listed are theoretical, as no confirmed detections have yet been made. However, it is abundantly clear that detection and study of this era of this part of the universe's history is rich with information about our cosmological origins, and could fill many of the gaps in our current knowledge.

Chapter 2

Interferometry

2.1 Brief Overview

An interferometer is any device which superimposes the waves from a coherent light source in order to gain information about the source itself. So what does that mean? Let's look at the most basic case of a Michelson interferometer. In this scenario, we have a coherent light source (typically a laser) pointing at a beam splitter. The splitter splits the light into two identical beams, which travel on separate paths, until they are recombined before entering a detector. The difference in the paths creates a phase difference between the beams. This phase difference is what creates an interference pattern, which is what then gives us the information we seek about the light source, which typically comes in the form of fringes.

What if instead of using mirrors and beam splitters, we built two identical small telescopes that were physically separated in space, then pointed them at the same astronomical source. Because they're not in the same spot but are separated by a "baseline", there must be a difference in the path lengths between the telescopes and the source. This is the fundamental idea behind radio interferometers. Now let's explore the mathematics.

In order to get a handle on the mathematics and theory behind astronomical interferometry, we're going to make some simplifying assumptions. We will consider the case of a two-element interferometer (that is, an interferometer with two antennas and one "baseline" between them) observing a very distant source (so the emissions from the source will come in the form of plane waves and the antennas will point in the same direction on the sky). This interferometer will be fixed in space - so, no rotation or motion of the antennas themselves. We will also be looking at just one frequency, so the signals coming in will be perfectly sinusoidal with one known wavelength. We won't be worrying about anything in the backend, so we'll say that we have no frequency conversions (an RF interferometer) with a single polarization and perfectly idealized electronics (perfectly linear, no amplitude or phase distortions, perfectly identical for both instruments, and no added noise). We'll also assume no propagation distortions, so the plane waves we observe from the source won't be disturbed by the ionosphere or atmosphere of Earth, and that the source is small enough in

angular size that we can approximate the sky as flat and two-dimensional.

What does that leave us? Two identical sensors that are separated by a vector distance $\mathbf{b}$ - this is our baseline. These sensors are both pointed at a quasi-monochromatic source of frequency ν, in the vector direction $\mathbf{s}$. Combining these fundamental numbers, we then get the key quantity $\tau_g = \mathbf{b} \cdot \mathbf{s}/c$, which is the geometric time delay. That's the extra time needed for the signal to reach the more distant antenna. This number will be important to us in order to correlate our signals. We can also find the phase shift in the signal by writing $\Theta = \omega\tau_g = 2\pi\mathbf{b} \cdot \mathbf{s}/\lambda$.

With this knowledge of the phase difference between the paths, we can write out the voltages received by each of the sensors, so we get $V_1 = E\cos[\omega(t - \tau_g)]$, because it has that extra phase delay from the baseline separation, and $V_2 = \cos(\omega t)$. In this case, the path lengths from the sensor to the multiplier are treated as being equal, so we don't need to add any extra phase terms. We then multiply our signals together, and take an average over time, which gives us an averaged product $R_C = P\cos(\omega\tau_g)$. This quantity is dependent on the received power $P = E^2/2$ and the geometric delay τ_g, and hence on the baseline orientation and source direction. We can rewrite R_C to make this relationship more explicit as:

$$R_C = P\cos(2\pi\frac{\mathbf{b} \cdot \mathbf{s}}{\lambda}) \tag{2.1}$$

Note that R_C is not a function of the time of the observation (so long as the source itself is not transient or variable), the physical location of the baseline (provided that the source is in the far field, which is always true of astronomical sources), or the actual phase of the incoming signals. All that matters is the relative phase between the sensors!

In order to get a better understanding of our observed response, let's rewrite some terms. Let us say that $\mathbf{b} \cdot \mathbf{s}/\lambda = u\cos\alpha = u\sin\theta = ul$. In this case, we are defining

$$u \equiv b/\lambda \tag{2.2}$$

which is the baseline length in units of wavelengths, and θ is the angle relative to the zenith. $l = \cos\alpha = \sin\theta$ is the direction cosine. We can then rewrite our response function as $R_C = P\cos(2\pi ul)$. We can now see quite easily that the longer the baseline, the more rapid the frequency of the response function R_C. This is what radio astronomers call "fringes".

We can also begin to see why we want to have many sets of antennas - each baseline will only give us information about one set of fringes. In order to reconstruct a full image of an extended source, we need to be able to observe more than one spatial frequency. The response from an extended source is obtained by summing the responses at each antenna to all emission over the sky, multiplying the two for each pair of antennas, and averaging. Assuming that the source itself is spatially incoherent (e.g. that the emission from one side of the galaxy isn't related to the emission from the other side), the averaging and integrals can be interchanged, giving us

$$R_C = \iint I(\mathbf{s})\cos(2\pi\nu\mathbf{b} \cdot \mathbf{s}/c)d\Omega \tag{2.3}$$

We can now see the relationship between what we are measuring to what we want to observe - we have linked the source brightness $I_\nu(\mathbf{s})$ to the even interferometer response R_C. To complete the image of the sky, we can observe the odd interferometer response R_S, which is the sinusoidal equivalent of R_C, by slipping in a 90° phase offset along one of the signal paths.

Now we can define a complex function $V = R_C - iR_S = Ae^{-i\phi}$ as our complex visibility from the two independent, real correlator outputs R_C and R_S, where $A = \sqrt{R_C^2 + R_S^2}$ and $\phi = \tan^{-1}(R_S/R_C)$.

We can now rewrite the complex visibility as an integral, giving us:

$$V(\mathbf{b}) = R_C - iR_S = \iint I(\mathbf{s}) e^{-2\pi i \nu \mathbf{b}\cdot\mathbf{s}/c}\, d\Omega \tag{2.4}$$

This is easily recognized as the 2D Fourier transform, when the right geometry is utilized. As it turns out, the earlier definitions of u and l are very convenient coordinates to use, and can be expanded to two dimensions to give us the (u, v) visibility plane and the (l, m) source plane[1].

Additionally, so far we have avoided mentioning any frequency dependence in this relationship or any intrinsic instrumental effects. The fact of the matter is that every astronomical array will have a frequency dependence, either from the response of the instrument itself or from the changing physics of the visible celestial sky (or, more likely, both). Therefore we must in fact calculate visibilities for all the frequencies within our science band (i.e. for each channel, meaning that there will be a level of imprecision and integration of each visibility across a known $\delta\nu$ of frequency space in the science band).

Moreover, we must also account for the fact that no antenna has perfect reception to the entire sky – rather, each antenna has some spatial sensitivity related to its own shape. This shape is often referred to as the "beam" or the "primary beam" of the antenna, and we shall denote it as $A(l, m)$.

Eq. (2.4) can now be rewritten with these coordinates like so:

$$V_\nu(u, v) = \iint I'_\nu(l, m) e^{-2\pi i(ul+vm)}\, dl\, dm \tag{2.5}$$

where $I'_\nu(l, m) = I_\nu(l, m) A_\nu(l, m)$. This is the van Cittert-Zernike theorem, a fundamental equation for interferometry, which relates the brightness of the distant source to the mutual coherence function (or visibility) via the 2D Fourier transform in a convenient set of coordinates for radio astronomy.

[1]In actuality, we don't use the uv-plane, but rather calculate from baselines $\mathbf{b}$ and source direction $\mathbf{s}$ directly, so as to avoid any complications or imprecision due to usage of the flat-sky approximation. See Appendix A for more information on the uv-plane and when it is an appropriate coordinate system to use.

2.2 Spatial Modes and Interferometric Sensitivities

As mentioned above in Section 2.1, interferometry gives you sensitivity to different spatially varying modes based on the physical separation of the antennas or telescope reflecting dishes making the observation. The bigger the separation, the faster the spatial variation observed on the sky, and therefore the higher resolution/smaller the object that can be observed.

It is through this knowledge that we are able to construct instruments that are specifically tuned to different spatial scales. For example, astronomers (and the general public) are fascinated by black holes and want to observe their inner workings. Black holes are very compact objects in the sky, so to be able to resolve them takes incredibly high resolution observations. Under the Rayleigh criterion (Eq. 2.6), radio astronomers can achieve fine resolution (i.e. small θ) by using high frequencies (i.e. small λ, of the order of less than a millimeter) and very large baselines (i.e. large B, on the order of thousands of kilometers).

$$\theta = \lambda / B \tag{2.6}$$

Alternately, if one wanted to observe fluffy galactic clouds or other extended structures, they would instead prefer to construct an interferometer using closely packed antennas and lower frequencies.

By constructing an array using a combination of differing baselines, one can fill in the sampling of the uv-plane. With complete sampling of the uv- plane, one can perform a simple 2D Fourier transform and perfectly recreate the image plane. This relationship between spatial frequency and images, or visibility and brightness, is known as the *spatial Fourier transform*, and is the backbone of all radio interferometry, from the reconstruction of cosmological power spectra all the way to the sophisticated synthesis imaging techniques described above.

In reality, of course, it is impossible to completely sample the uv-plane and recover a perfect image. We must therefore design our instruments to be maximally effective at the observations we wish for them to make. In the cases of general purpose instruments like the Very Large Array (VLA), that means designing the instrument to be very flexible – covering a broad range of frequencies, minimizing redundancy in the baselines, and using different array configurations to better sample different regions of the uv-plane.

However, for smaller scale instruments, astronomers generally wish to build something which is very specifically tailored for the observation they want to be making, leading to creative and highly unique array configurations that make use of the spatial Fourier transform to the best of their ability.

Spatial Fourier Transforms

Much as we can think of the relationship between time and frequency as a Fourier pair, we can also relate the physical separation of the antennas (i.e. the "geometric time delay" τ_g) and the spatial frequency.

Consider the variable u, which is defined as the baseline separation of two antennas measured in wavelengths in Eq. (2.2). Based on Eq. (2.1), we also know that $R_C \approx \cos(2\pi ul)$, meaning that the number of whole fringes imposed across the sky for any given separation will be $N_f = 2u$.

This in turn means that a pair of antennas separated by u wavelengths will be most sensitive to objects with an angular scale of about $\theta = 1/u$, according to Eq. (2.6).

One can relate this to the idea of spherical harmonics, with the harmonics providing us the (l, m) coordinates of our observed brightness, providing us some context for the second member of our spatial Fourier pair. We can thus start visualizing the physical meaning of "spatial variance" and "spatial frequencies".

We can do so by rewriting our interferometric visibility in terms of spherical harmonics. Let's begin by rewriting our visibility equation into the form seen in Eq. (2.4), now factoring in the primary beam and integrating over the full celestial sphere.

$$V(\nu) = \int I(\mathbf{s})A(\mathbf{s})e^{-2\pi i\nu \mathbf{b}\cdot\mathbf{s}/c}\, d\mathbf{s} \tag{2.7}$$

where $I(\mathbf{s})$ is the sky brightness, $A(\mathbf{s})$ is the primary beam of the antenna, and the exponential term is the interferometric "fringe". Now, much in the way that any signal can be decomposed into an infinite series of Fourier frequencies and amplitudes, we can rewrite the terms of Eq. (2.7) to be expressed as a sum of spherical harmonics.

$$I(\mathbf{s}) = \sum_{l,m} I_{lm} Y_l^m(\mathbf{s}) \tag{2.8}$$

and therefore the visibility equation becomes:

$$V(\nu) = \int \Big(\sum_{l,m} I_{lm} Y_l^m(\mathbf{s})\Big) A(\mathbf{s})e^{-2\pi i\nu \mathbf{b}\cdot\mathbf{s}/c}\, d\mathbf{s} \tag{2.9}$$

So now the question is simply: does the integral of the zeroth mode (i.e. the global signal) vanish or not. This term can be written as:

$$V_0(\nu) \equiv I_{00}(\nu) \int Y_0^0(\mathbf{s})A(\mathbf{s})e^{-2\pi i\nu \mathbf{b}\cdot\mathbf{s}/c}\, d\mathbf{s} \tag{2.10}$$

We know that $Y_0^0 = \sqrt{1/4\pi}$, so the remaining question of interest basically boils down to whether or not the beam can break the inherent symmetry of the fringe term, leaving us with a non-zero $V_0(\nu)$.

ROPE IN TOP HAT-BESSEL DUALITY HERE – WHAT IF BEAM IS A TOP HAT? SHOW SOME EQUATIONS

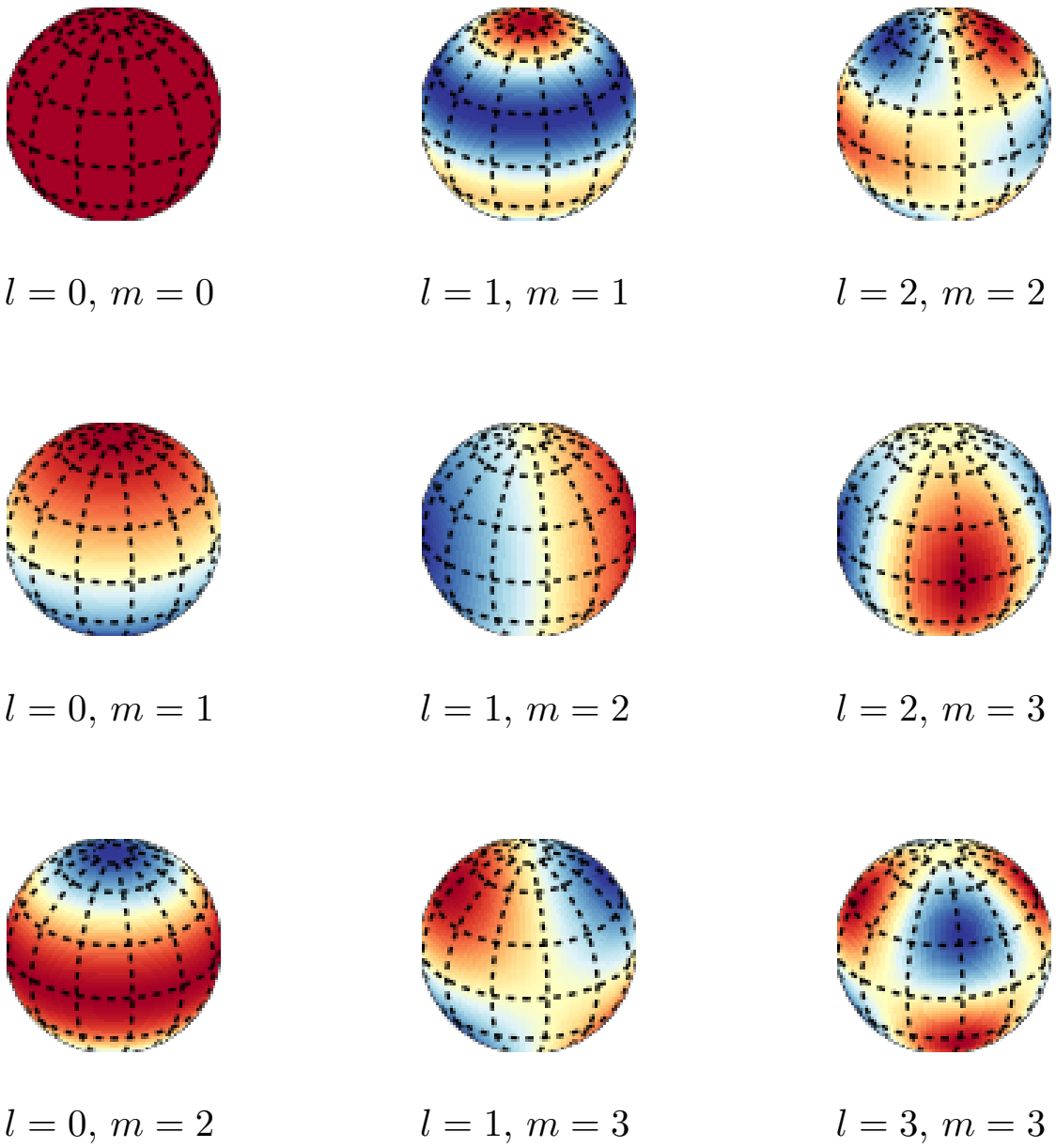

Figure 2.1: Above, we see a collection of the low-order spherical harmonic functions. This can help us begin to visualize what, physically, the spherical harmonics are and how they can be used to parse spatial information observed on the sky from an interferometer.

2.3 Observing the Spatial Monopole with an Interferometer

At this point, it is a fair enough question to ask how exactly we intend to use an interferometer to observe a spatially invariant signal. Everything we have stated above indicates that interferometers see *changing* signals – they observe the spatial variance that they are sensitive to based upon the separation of the antennas and the frequency they are observing at. They are inherently AC circuits. The one thing they are explicitly not meant to do is to observe what is effectively a DC tone.

So how exactly is this supposed to work?

Well, it turns out there's a couple of things in our favor here. The first thing, as addressed in Presley et al. (2015), is that we're on earth and can't actually see a monopole from the sky – the horizon gets in the way. Furthermore, the antenna itself has a directionally dependent beam, introducing an additional layer of spatial variance. Therefore, what in reality is a monopole signal from the entire universe is instead observed with a spatial cut-off – it's a top-hat. Or, more accurately (with the addition of the primary beam A), it's a bowler hat. And, most importantly for our goals, a top-hat signal doesn't necessarily integrate to zero and therefore may be observable with an interferometer (Venumadhav et al. 2016).

That being said, a top-hat signal that spatially broad still isn't easily observable with an interferometer. From our knowledge of Fourier transformed, we know that a broad spatial cut-off translates into a narrow spread of powers in the visibility domain – i.e. most of the monopole power will remain in very broad, long and low spatial modes. If we want to truly convert the monopole into a signal that we can get at with an interferometer, we're going to have to constrict the scale of our spatial top hat.

What we need to do is artificially push our monopole term into higher modes – modes that we are in control of. Or, in Fourier terminology, we need to apply a top-hat function to our monopole signal.

In doing so, we will generate a visibility sensitivity in the shape of a sinc function – meaning we will have sensitivity to our monopole term in many Fourier modes, rather than just in the $(0, 0)$ or $(0, 1)$ modes. If we control the shape of the top hat imposed, then we know the shape of the sinc function, meaning we can calibrate exactly what our monopole sensitivity should be at any given point in the uv-plane.

So now the question is simply how can we raise the horizon that our antennas see? One option would be to literally raise the horizon – either find or manufacture a deep valley for them to reside within. This would probably be challenging to do well – digging a valley for the whole array would undoubtedly be expensive, and it'd be very hard to find a naturally occurring, rotationally symmetric valley (particularly one deep enough to actually meaningfully raise the horizon of our antennas).

So we must find a way to artificially raise the horizon of our antennas. Moreso, as described in Venumadhav et al. (2016), we must either allow our antennas to freely cross-talk (thereby eliminating the vast majority of benefits gained from using an interferometric

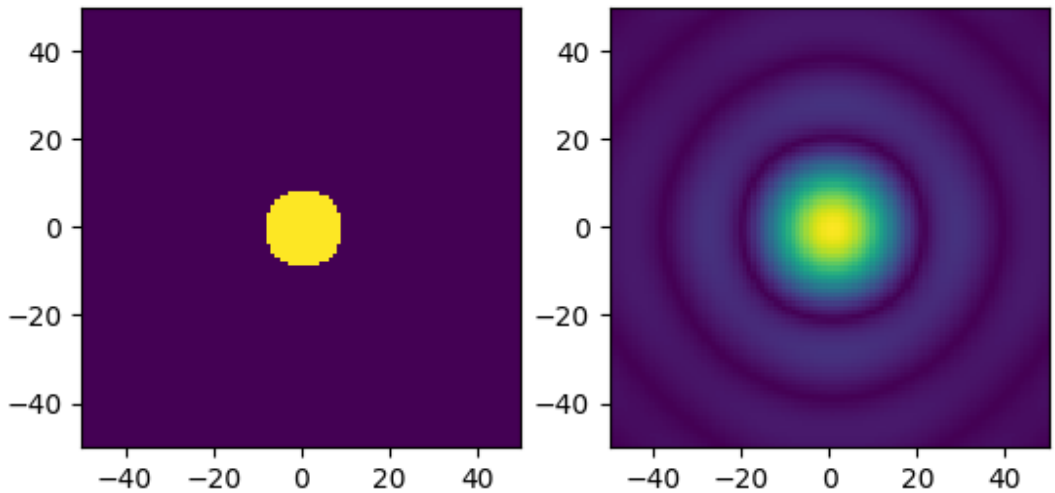

Figure 2.2: This figure shows the Fourier relationship between the two-dimensional top hat function and a Bessel function. This image can be thought of as an idealized cartoon of the aperture and visibility planes of our proposed interferometer. On the left, we see the imposed top-hat, where the yellow portion would be the portion of monopole sky visible to the antenna and the blue would be the perfect absorber. On the right, we have performed a two-dimensional Fourier transform to convert into the visibility plane (i.e. to see the spatial modes to which we are observationally sensitive), and we see this rippling function centered around the zero-spacing mode. WRITE DOWN MATHEMATICAL RELATIONSHIP AS WELL

setup) or we must introduce a source of noise from lossy components (e.g. the ground or other signal absorbers, rather than reflectors or transmitters) in order to maintain a sensitivity to the global signal. As described in Section 2.1, the more closely spaced your elements, the larger the spatial scales on the sky your instrument will be sensitive to. We therefore know that we are going to be using a very closely packed array, which will make our system very prone to cross-talk. If we want to avoid that, then we'll have to find some way to ensure that the antennas don't see each other in addition to seeing less of the sky.

All of which leads us to the construction of thin absorptive walls between the antennas – introducing a new horizon in how the antenna sees the sky and maintaining the independence of each antenna's signal from its very nearby neighbors. In order to maximize our sensitivity to the global signal, we will want the absorbers used to be highly efficient at dissipating energy across our frequency spectrum (Venumadhav et al. 2016). This will provide us will a strong "edge" in how our antennas see the sky, in turn creating maximal Fourier leakage into higher modes and best enabling us to make a successful observation of the reionization monopole signal.

Chapter 3

Overview of the Theory of HYPERION

3.1 Absorber – A New Approach to Monopole Interferometry

If you were to wander onto almost any given radio telescope currently active in taking observations, you're almost certain to find some kind of reflective material underneath the antennas (either in the form of a ground screen or a reflective dish). One thing you're not likely to find is any kind of absorptive material – we as astronomers are already fighting an uphill battle on attaining the very fine sensitivities needed to detect celestial sources, we really need all the photons we can get.

However, it is not unheard of. While absorbers have never been used in the element design of a reionization project to date, they have been used by cosmic microwave background (CMB) experiments. Absorptive structures, or baffles, to control pickup from outside the main beam, which can be a source of systemic errors Essinger-Hileman et al. (2016). By surrounding the receiver with an absorptive material, rather an a reflective one as seen in most standard radio telescope designs, one can better control the exact signal that will be seen in the sidelobes of the beam, and thereby better calibrate the system in turn.

This same principle applies in the case of a monopole interferometer, where use of an absorber can not only be beneficial but actually fundamental to the design of the array despite the microscopic signal we aim to detect. By controlling what each antenna sees on the sky, we can accurately calibrate our system and ensure that our reionization signal is indeed signal and not instrumental noise.

Practical Instrumentation

As discussed in Chapter 2, one of the fundamental requirements of a monopole interferometer is close spacing of the antennas, in order to maximize reception of the global sky mode.

However, this close spacing also predisposes the instrument to cross-talk. As discussed in Venumadhav et al. (2016), this isn't necessarily a bad thing – cross-talk is one of two ways that an array of antennas can maintain a sensitivity to the monopole. Each individual antenna will broadcast its reception of the monopole to its neighbors, and that reception will correlate. In this case, one will have a direct view of the monopole term, as you will be correlating the zero-spacing mode seen by one antenna with the zero-spacing mode of another, thus providing the necessary sensitivity to the global signal.

However, that also means that instrumental noise will be broadcast and correlated between antennas, vastly diminishing the useful properties of the interferometer and maintaining many of the pitfalls of single-dish instruments. The risk here comes in the calculus of calibration for the instrument. In particular, it is difficult to properly calibrate the correlated noise between elements as it has a noise bias. This bias means that, while we observe more of the true signal, we also no longer are able to integrate down the instrumental noise, essentially placing a DC offset into our system. The exact value of this offset is a function of frequency and of the exact qualities of the instrument, and will likely vary from element to element. If it is not perfectly calibrated and subtracted off from the data, then traces of this bias will remain in the final data and can easily be mistaken for true science.

So we'd like to avoid cross-talk and other sources of correlated noise between elements as best as we can, while still maintaining a sensitivity to a correlated monopole signal. The only other way for an interferometer to have the capacity to observe the monopole is through the presence of dissipative elements, such as absorbers and/or the ground. Without cross-talk or dissipative elements, the monopole term will integrate to zero in every non-zero spatial mode, making the interferometer completely insensitive to the global signal Venumadhav et al. (2016).

One way to manage cross-talk it to pack the space between antennas with absorber – with a high-enough quality absorber, we can essentially make the antennas invisible to each other by just placing a tall enough wall between them. Ideally, this material would be quite physically thin, so that these absorber walls wouldn't force us to spread the shape of the array at all, thus maintaining a sensitivity to the spatial monopole of the reionization global signal.

In order for this to work, the absorber needs to meet some basic criteria. Most importantly, it will need to be at least optically thick enough that antennas on opposing sides of an absorber wall will not observe the same noise signal from the absorber. If the noise observed from the absorber is coherent between elements, then we will fall into the same pitfalls that arise from cross-talk between elements, described above.

Additionally, the absorber walls need to be shaped in such a way that signal won't reflect and bounce over the barriers – if signals are able to diffract off of one antenna and into the other, then there will still be cross-talk and our calibrations will be flawed. For this reason, we won't be able to build straight walls with sharp cutoffs. Rather, we want to build our walls in a way that signal gets trapped into the absorber or angles out of the array entirely. Ideally, we'd like to build our walls with some kind of pyramidal structure (to capture and dampen the signal within the absorber), and with a curved roll-off at the top edge (to prevent

reflections off of the baffle into multiple antennas).

Manipulating the Spatial Monopole

Another benefit to the use of absorber in our array is how we can use it to manipulate the instrument's sensitivity to the monopole. As discussed in Sec. 2.3, by applying a spatial windowing function to our monopole signal, we can increase our interferometric sensitivity to the global signal. The absorber can impose this windowing function by creating a spatial temperature change in the absorber's field of view, increasing the harmonic content of the monopole signal by imposing non-isotropic terms.

Let's take a closer look at how this is to actually work. In a perfect world, our absorbing material would be 100% effective and no information could be transmitted through it – it would absorb all incident light and re-emit it as thermal radiation. That means that, as per Fig. 3.1 and ignoring the effects of the antenna beam shape, the antenna would see the sky up until an angle of θ off of zenith, and then it would see a perfect blackbody matching the ambient temperature of the array everywhere else.

One way to understand the absorption of the blackbody would be to think in terms of optical depth, and the above case is one in which the absorber has an optical depth of $\tau = \infty$. This thinking also enables us to begin to understand more realistic scenarios, where we don't have perfect absorption between our antennas.

$$I_{obs}(\theta) = I_{sky}\ e^{-\tau_\theta} + S_{abs}\ (1 - e^{-\tau_\theta}) \tag{3.1}$$

where I_{obs} is the observed sky brightness, I_{sky} is the sky brightness, S_{abs} is the thermal brightness from the absorber, and τ is the optical depth of the absorber. This equation is a variation on the radiative transfer equation, where the sky is our source and the absorber is the medium through which the radiation is travelling.

In this quantitative construction of the reception of an element, we can see that the strength of the absorber determines the strength of the spatial cutoff – particularly, in the case of a poor absorber, the above equation shows that there will be a great deal of sky leakage into the "horizon". In particular, for reionization studies, this will be problematic due to the brightness of the sky at these frequencies from galactic synchrotron emission. So a weak absorber will barely put a dent in the sky brightness, diminishing the effectiveness of the imposed window, and keeping the reionization global signal power in the lower, harder to detect spatial modes.

Additionally, if the quality of the absorber is poor, this can increase the confusion between inherent sky structure and windowed monopole sky. Consider the fact that the sky itself will not be a perfect monopole and will therefore have spatial structure. If the quality of the absorber is poor, then more of that structure will be visible across the whole sky. This will exist in addition to the characteristic spatial sensitivity of the monopole portion of the sky. This mixing of intrinsic sky structure and imposed sky structure must be handled carefully, and having a high-performing absorber can help us to better control those parameters.

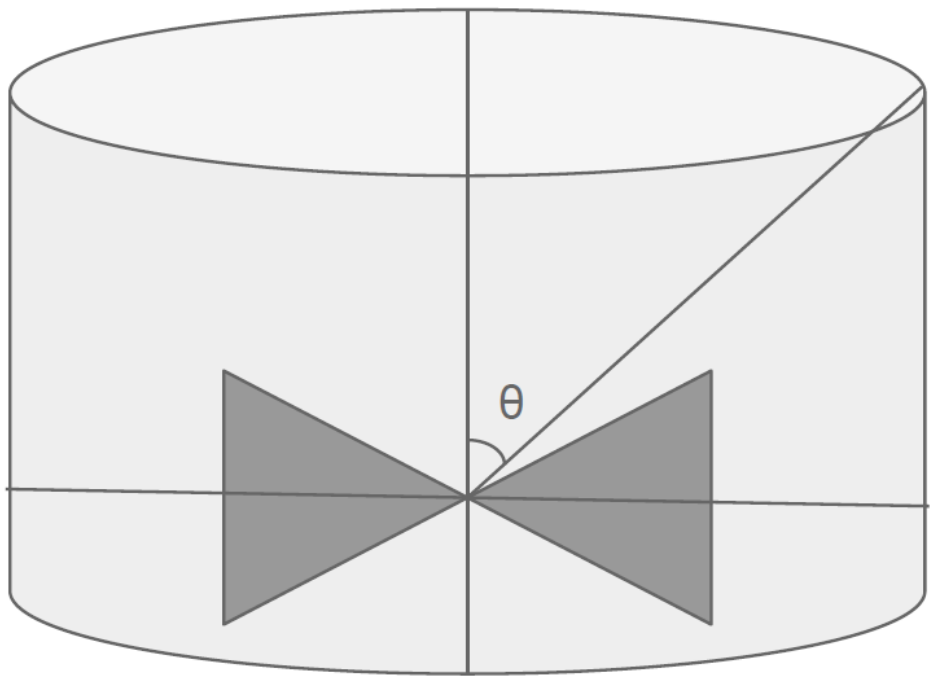

Figure 3.1: This cartoon shows the basic structure of the proposed absorber walls. Each antenna in the array will be circled by a cylinder of absorber material, creating a uniform temperature cutoff in the antenna's reception of the sky. By increasing the height of the wall, we can change the cutoff angle of the reception of the sky, thereby shrinking the spatial windowing and pushing more of the monopole to higher spatial modes.

Finally, if the absorber is optically thin, then antennas on either side of an absorber baffle will see coherent signal coming from the absorber, contributing to an overall noise bias that may be hard to calibrate for.

3.2 Overview of the Instrumental Design

Let us now consider the design of our interferometer itself. There are two key areas of interest to us: how our sensitivity to the monopole varies with the separation between antennas, and how it changes in the presence of different absorber structures and materials. Another way of viewing it would be: how do the characteristics of the individual elements and of the array design affect our ability to make this measurement.

Let us first consider the array design, i.e. baseline separations. Intuitively, we expect that the sensitivity to the global signal will be maximized with the smallest baseline separations, which correspond to a position in the uv-plane close to the origin, or the zero-spacing mode. The trade-off of this, from a design perspective, comes in the difficulty of ameliorating cross-talk in a densely packed array. We want to optimize our array design to space our antennas as loosely as possible while also maintaining workable sensitivity to the monopole term, as this will best enable us to mitigate systemic problems in our instrument and perform a successful experiment.

The next step is to add the absorber, which can essentially be treated as a modification to the antenna's beam. This calculation is done using Eq. (3.2),

$$B(\theta,\phi,\nu) = 10^{\alpha(\nu)/20}\Big(\frac{1}{2}+\frac{1}{2}\tanh\Big(\frac{\theta-(\frac{1}{2}-\theta_0)}{a}\Big)\Big)+\Big(\frac{1}{2}-\frac{1}{2}\tanh\Big(\frac{\theta-(\frac{1}{2}-\theta_0)}{a}\Big)\Big) \quad (3.2)$$

where $\alpha(\nu)$ is the absorptivity by frequency of the absorber, θ_0 is the cutoff angle of the structure (i.e. θ_0 is the height of the absorber walls), and a is the smoothing parameter that blends the transition between the absorber and the sky.

This term is then combined with the antenna beam, giving us Eq. (3.3).

$$A'(\theta,\phi,\nu) = A(\theta,\phi,\nu)B(\theta,\phi,\nu) \quad (3.3)$$

One thing to note about our particular experiment is that there is no need for cryogenic cooling. As mentioned in Section 1.1, the expected values for the 21 cm reionization global signal are far, far fainter than that of the ambient emission from our own galaxy. In the proposed science band for HYPERION, we expect the galactic synchrotron component of the sky brightness temperature to range from about 650–3700 K (Haslam et al. 1982). This is, at best, 40,000 times brighter than the reionization signal that we are seeking.

This also means that there is no need to cool the absorber baffles – the sky is bright enough on its own to easily dominate the overall system temperature, so leaving the absorbers warm has no significant effect (Kundert 2016),

Chapter 4

Overview of the Logistics of HYPERION

We must now find a way to test our hypotheses about building a monopole-sensitive interferometer. Ideally we would do this in multiple steps, graduating from tests that use the fewest resources up to the most expensive tests, and would conclude with a full deployment of the array with which to observationally test our ideas and attempt to make a measurement of the monopole reionization signal.

This leads us to a natural starting point: to build a simulation of our array. This can be done cheaply and relatively quickly, and can give us a sense of whether or not this idea has any potential merit.

4.1 Methodology of Simulation

Fundamentally, we will be doing all the same steps that have been laid out in the previous three chapters. We will create a model sky and a model array, and then calculate the visibilities for each baseline separation of that array. We will then examine these visibilities to see if we have any sensitivity to the monopole term at all, and if so what form they take.

For our simulation, we first import a model array, which enables us to carry around a known geometry and baseline separations, along with individual antenna beam patterns and accessible frequencies. With this information and the previously made sky maps, we are now able to calculate our visibilities across many frequencies by using Eq. (2.4).

More importantly, the antenna beam information within the model array is itself a convenient way to import absorbers into the simulation. Essentially, within the context of the simulation, the absorbers act as a modification term on the beam pattern, changing the way that each individual antenna sees the sky.

Antenna Design and Primary Beam

TALK ABOUT SARAS OR SOMETHING IDK, BENEFITS OF FAT DIPOLE (FREQUENCY INDEPENDENCE)

To start, we need a beam. HYPERION uses SARAS-style fat dipole antennas in our instrument, which means we will be using a frequency-invariant dipole beam pattern in our simulation to match (Patra et al. 2013). This is the base beam model used throughout the simulation, calculated using Eq. (4.1).

$$A(\theta, \phi, \nu) = \cos\left(\frac{\frac{\pi}{2}\cos\theta}{\sin\theta}\right) \tag{4.1}$$

Absorber Baffles

Now that we have a baseline antenna beam, we can begin the modification process. The effective antenna beam be calculated using equations (3.2) and (3.3).

In the construction of the absorber baffles within the simulation, the parameters we can play with are the absorptivity of the material (i.e. how much attenuation does the absorber provide at each frequency), the height of the absorber walls, and how smooth the transition from absorber to sky is.

So the first question is: how absorptive is our absorber at each frequency? To date, we are still relatively early in the testing of our hypothesis that absorber walls or "baffles" between antennas will enable us to better observe the spatial monopole with an interferometer. There have been two main sets of tests performed so far – one in-lab test to measure the absorptivity of various proposed materials, and some brief field tests to gauge the effectiveness of our absorber at mitigating cross-talk between antennas.

The in-lab test was, in essence, a simple antenna return-loss measurement. To conduct the measurements, we started by constructing a large (i.e. 4.5' cube) Faraday cage out of wood and chicken wire, and placed an antenna at its center. From this setup, we could perform a simple return loss measurement and see what the maximum power return to the antenna is.

We could then line the cage with various absorptive materials and take another return-loss measurement, this time with (ideally) much of the power absorbed by the absorber, and see how effective each material is at dissipating energy within our science band. One such measurement is shown in Fig. 4.1, featuring our most promising absorber candidate material, ferrite tiles.

As can be easily seen in the figure, the ferrite tiles have a decent absorptivity profile across the band, and an excellent absorptivity around 120 MHz. However, as described in Section 1.2, the global signal of reionization is rich with physical information that is uniquely tied to its changing amplitude by frequency. The kinds of variations that we see in the absorptivity across the band are dangerous for the well-being of our experiment, as they could translate to tricky or uncertain calibration of our final instrument. We want to ensure that almost everything beyond the global signal has simple and well-defined relations

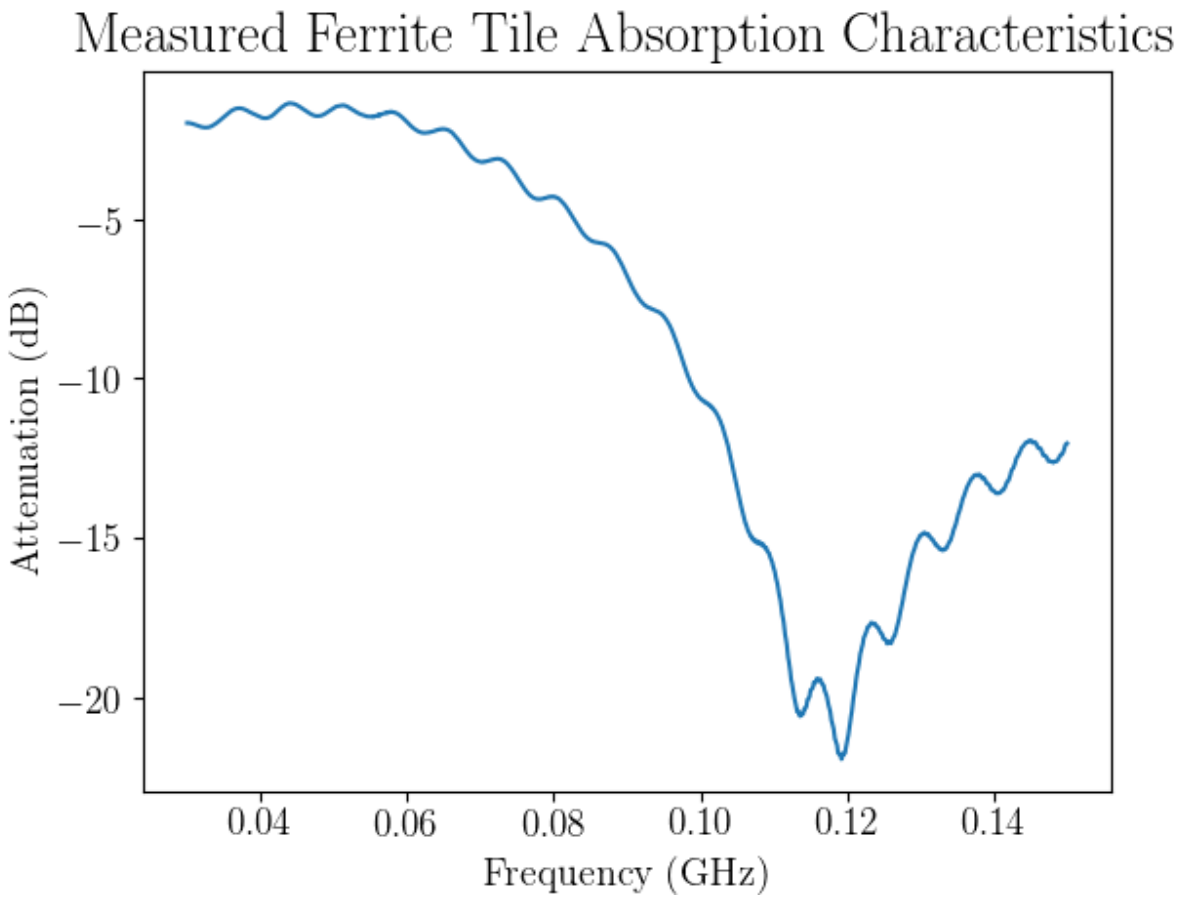

Figure 4.1: Here we see the results of a closed-box return loss measurement taken with a densely packed (i.e. 9×9 tiles per wall) configuration of ferrite tiles, evenly spaced along the walls of the testing Faraday cage. The ripples are an artifact from the testing setup, and not inherent to the performance of the ferrite itself. As can be easily seen, the Ferrite performs much better at the high range of our science band, and is optimized around 120 MHz. While this material has the best performance out of all the materials we have looked into so far, we would ideally prefer a material with a more even absorptivity across the band, so as best to avoid inadvertently adding ripples or structure to our sky observations.

to frequency (e.g. the synchrotron galactic sky, which is well described by a power law), in order to best understand our signal and be sure that instrumental idiosyncracies aren't being mistaken for true signal and science. As such, we would strongly prefer an absorber (or combination of absorbers) that has a more uniform performance across the science band.

That being said, Fig. 4.1 appears worse than it actually is. The ripples seen in the figure are simply an artifact of the testing setup, and not inherent to the performance of the ferrite itself.

However, there is one additional disclaimer to be made about the measured ferrite absorption. We are assuming that the ferrite absorptivity is the same in all directions – that the incident angle of the radiation has no effect on its absorptive properties. This isn't necessarily true, but rather is reflective of the limitations of our testing environment, which fundamentally averaged over all directions of incidence.

Additionally, the ferrite tiles are among the most expensive of the materials we investigated. Even with a very close spacing and therefore relatively small baffle structures, the costs of acquiring enough ferrite to create an array quickly becomes overwhelming to the budget.

Other candidate absorbers include mats of Zotefoam Plastazote®, the AEP-EM low-frequency pyramidal foam absorber from DJM Electronics, and the creation of a grid of resistors designed to match with the free-space impedance (Mahesh et al. 2015). The Zotefoam was appealing due to its low cost compared to the pyramidal foam and ferrite tiles, but unfortunately its performance seemed to scale in proportion to its price tag. The pyramidal foam performed slightly better, but seemed to feature more reflections than the ferrite and overall had a lower absorptivity performance than the ferrite, despite a nearly identical price tag per square foot of coverage. The resistive mesh is still an attractive idea, as it would only cost us an ungodly amount of effort to put together and about $10 worth of resistors. Unfortunately, at the time of writing, only a very introductory level of investigation has been put into the resistive mesh idea, so nothing conclusive can be said about its performance as an absorber material.

At this point in time, there really haven't been any meaningful field tests upon which to report. However, the most important things for us to investigate in the field would be a) ability of the absorber to mitigate the cross-talk between antennas and b) the efficacy of the baffles' ability to impose a spatial temperature variation from the antenna's point-of-view and how that efficacy evolves over frequency.

In Fig. 4.2, we see one possible arrangement of the absorber materials in order to assess the ability of the absorber at mitigating cross-talk between antennas. In order to perform this test adequately, one would need to take two measurements in the same radio environment – one without the absorber between the antennas, in order to gauge the baseline level of cross-talk, and one with the absorber between, to measure the improvement in power leakage.

Presently, we don't have any field results for how effective the absorptive walls are at mitigating cross-talk between antennas. The current iteration of the simulation assumes zero cross-talk between antennas, i.e. all sensitivity to the monopole comes from the presence of the dissipative absorber walls (Venumadhav et al. 2016).

Figure 4.2: Shown here is a simple diagnostic field set-up that could be used to evaluate an absorber's ability to mitigate cross-talk between elements. Here we used a densely-packed configuration of ferrite tiles that have been propped up on some of our pyramidal foam absorber for additional height.

We also haven't tested how the absorber behaves at the edges. Most importantly, we don't have a good grasp on how big of a problem diffraction over the top of the baffle walls is, and we don't have a model of the smoothing parameter a from Eq. (3.2) or how it evolves with different baffle shapes. For the simulation, we have assumed that there is no diffraction and that the roll-off in absorber effectiveness is fairly sharp with $a = 0.01$.

ROLL-OFF IS FIRST ORDER APPROXIMATION OF DIFFRACTION, WE DON'T KNOW HOW EXACTLY TO PARAMETERIZE a, DISCUSS HOW DIFFERENT a VALUES IMPACT GLOBAL SIGNAL RECOVERY

In all cases, the next investigative step would be to create a full electromagnetic model of the combined antenna-absorber baffle system. Not only would this allow us to further investigate diffraction effects, it would also allow us to better understand the mutual coupling between the absorber and the antenna.

Array Parameters

Next, we must construct our model array. Basically, this means we must decide on the placement of our antenna-absorber elements. Our intuition tells us that the closer the elements are spaced to each other, the more sensitivity we will have to the monopole. But, of course, we don't yet know what the final baffle design for the elements is, and therefore we don't know how much space we will have to leave between elements.

At this level of the simulation, we are simply trying to determine what level of sensitivity we can expect across our full science frequency band at many different separations. We have chosen to test six possible separations: 1.5 m, 3 m, 4.5 m, 6 m, 9 m, and 12 m. This corresponds to $\lambda/2$, λ, $3\lambda/2$, 2λ, 3λ, and 4λ for a frequency of $\nu = 100$ MHz, approximately the center of our science band.

Modeling the Sky

CITE HEALPIX, GORSKI

Finally, we need something to actually observe. We can construct a model of the sky using the AIPy Healpix tools, generating maps of the sky at multiple frequencies and storing them in bundles. These maps are contained and can be indexed by coordinates, making them easy to use for simulating observations and interferometric visibilities.

There are three things we hope to learn from our simulation, each one building upon the others.

1. Can we observe a monopole sky using an interferometer?

2. Can we see the reionization monopole in our interferometric observations even with very bright foregrounds?

3. Can we tease apart the monopole signal from the higher order, very bright foreground terms?

So fundamentally, we must be able to generate model skies for at least three cases: a monopole sky that models the frequency dependence and amplitude of the predicted reionization global signal, a monopole sky with a synchrotron frequency dependence, and a full global sky model for each frequency in our science band.

First off, we want to be able to model the monopole reionization signal. To do this, we will first generate a Healpix map filled with a flat brightness of 1 K for each frequency we want to simulate. We will then use the Accelerated Reionization Era Simulations (ARES) code developed by Jordan Mirocha to calculate the brightness temperature of the 21cm global signal at each frequency bin (Mirocha 2014). Finally, we will scale the brightness of each map by the temperature calculated for its frequency, giving us a flat sky with an evolving brightness by frequency.

The same process can be used to generate a monopole synchrotron sky. In this case, the temperature at each frequency bin can be calculated via simple power law:

$$T(\nu) = T(\nu_{150})\left(\frac{\nu}{\nu_{150}}\right)^{-\beta} \tag{4.2}$$

For our synchrotron sky, we have used the numbers presented in Rogers & Bowman (2008), which lists a synchrotron sky brightness temperature of $T = 237$ K at $\nu = 150$ MHz and a scaling factor of $\beta = 2.5$. These numbers give us a galactic synchrotron brightness temperature of $T_{synch} = 3700$ K at $\nu = 50MHz$, which is the lowest frequency in our science band and therefore the brightest synchrotron bin.

Finally, we want to be able to generate realistic sky maps with structure. We can do this using global sky models at multiple frequencies, such as those first presented in Haslam et al. (1982).

Chapter 5

Sensitivity to the Monopole Sky

Now all that remains is actually answering the question of whether or not this could work. Can a traditional interferometer actually pick up a global sky signal? Can we manipulate that sensitivity using the strategic placement of absorptive materials around our antennas? And finally, and most importantly, can we actually understand the signals that we are sensitive to in order to accurately interpret our data, thereby actually observing the global signal of reionization?

5.1 Simulated Visibilities

Fundamentally, we are simply trying to calculate the visibility to the sky with a specific array set-up. We can describe this mathematically using the interferometric framework developed in Eq. (2.7). For the specific case we are investigating of a monopole sky and with absorptive baffles modifying the antenna beam, we get Eq. (5.1):

$$V(\nu) = T_{global}(\nu) \int A(\mathbf{s}) e^{-\tau(\mathbf{s},\nu)} e^{-2\pi i \nu \mathbf{b}\cdot\mathbf{s}/c} \, d\mathbf{s} \tag{5.1}$$

where T_global is the temperature of the monopole sky, $A(\mathbf{S})$ is the antenna beam, $e^{-\tau(\mathbf{s})}$ is the spatial absorptivity, which is a function of direction and frequency. Here we see that the monopole sky has a convenient quality in that its lack of spatial information allows us to pull it out in front of the integral as a constant factor.

For our array, we will be considering the following set of perfectly east-west baseline separations: $\mathbf{b} = [0, \lambda/2, \lambda, 3\lambda/2, 2\lambda, 3\lambda, 4\lambda]$ for a $\lambda = 100$ MHz.

Let's start by investigating the first question. Is an interferometer sensitive to the monopole sky? As described in Chapter 4, this can be be simulated, we just have to set our parameters appropriately.

We can begin with a very simplified proof-of-concept case. We will construct an array with no absorbers and a flat terrestrial horizon. Additionally, we will have beams with perfect receptivity in all directions, and a sky temperature of exactly $T_{global} = 1.0$ K across

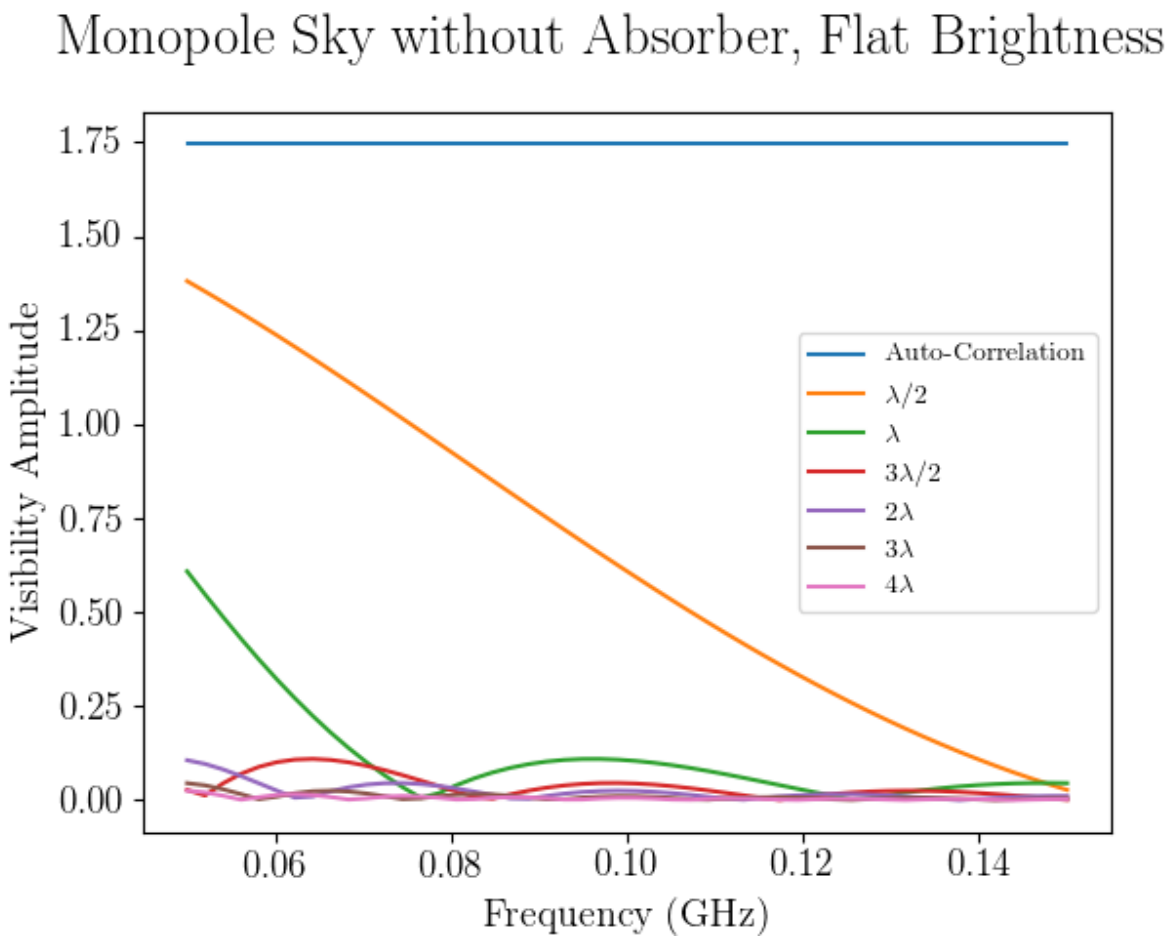

Figure 5.1: Shown here is the absolute value of the visibility of a spectrally flat monopole sky versus frequency. In this case, there are no absorptive baffles, just the terrestrial horizon. As can be seen already, the interferometer does have non-zero sensitivity to the monopole, though it is plainly clear that the autocorrelation term (shown in blue) is more sensitive than any of the non-zero interferometric baseline pairings.

our entire observational band. This will be our most basic unit test – something with which to check our intuition against and prove that the idea behind HYPERION is sound.

As expected and as can be easily seen in Figures 5.1 and 5.2, all ground-based interferometers have a non-zero sensitivity to the monopole mode of the sky. Similarly, we also find that the further we stray from the zero-spacing mode (i.e. as the number of wavelengths of separations increases), sensitivity to the monopole also quickly evaporates.

But this simple unit test tells us much more than just the fact that HYPERION is feasible after all. We can also begin to see a characteristic shape of the sensitivity in the *uv*-plane, with peaks and nulls placed at regular intervals in *uv*-space. The predictability of this shape

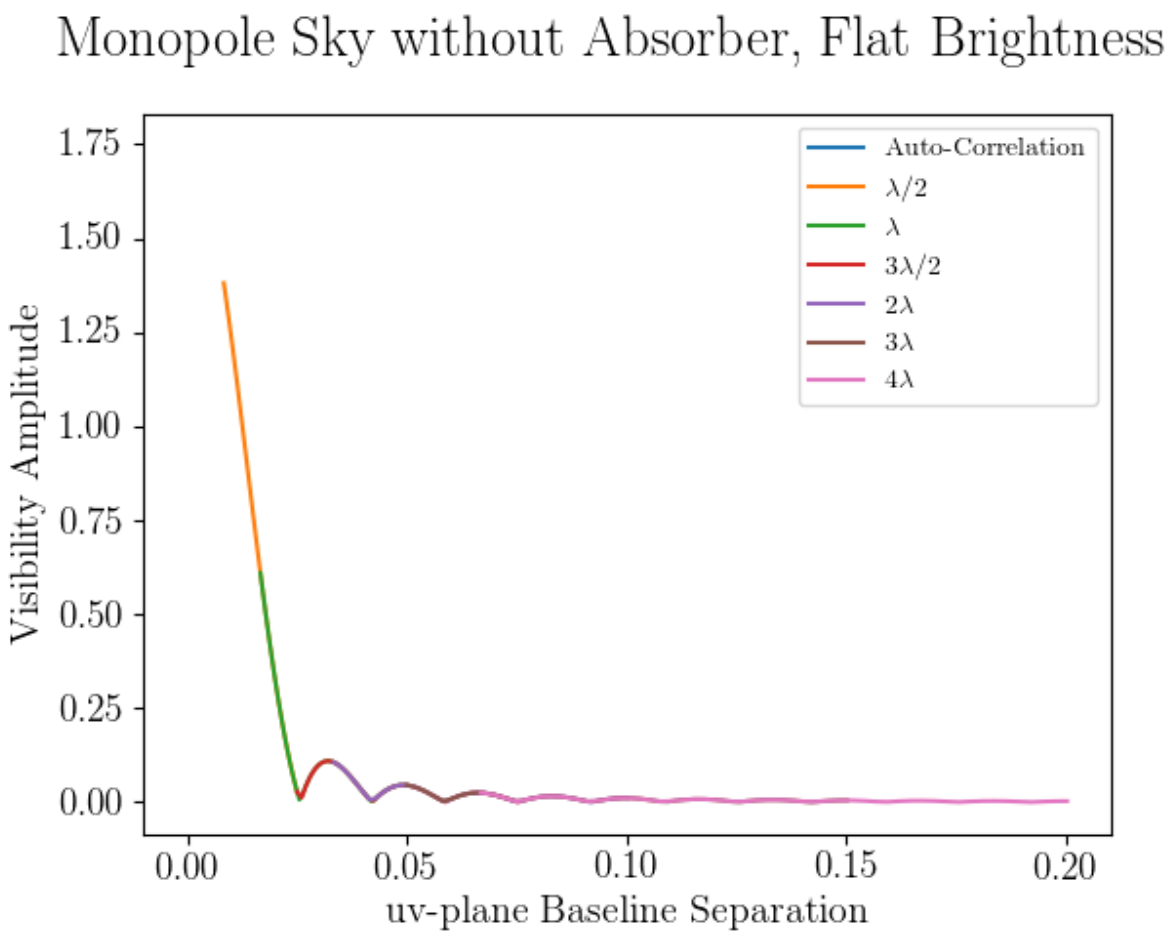

Figure 5.2: Shown here is the absolute value of the visibility of a spectrally flat monopole sky with no absorber walls versus uv-baseline. As can be seen already, the interferometer has a non-zero sensitivity to the monopole at non-zero baseline separations.

could allow us to use it as a calibration tool, if properly understood. In particular, it could be a valuable way to remove leakage from non-monopole terms into our signal. Given that this characteristic shape derives only from the monopole sky and the shape of the beam, we know that any observational deviations in this shape must come from the sky rather than the system. Therefore, it may be possible to use this information as a way to filter out non-monopole terms from the sky, thus ensuring that we won't mix up spectral wiggles from the combination of various non-monopole sky sources with our expected wiggly reionization global signal, as seen in Fig. 1.1. Instead, we can, effectively, select just the monopole terms of the sky – the galactic synchrotron background and the reionization global signal – thus ensuring that the only terms we're left with have simple relationships with frequency that can be easily parsed from the frequency-independent evolution of the reionization term.

Additionally, this characteristic shape could enable us to do some weighting of our observational data. By knowing exactly what modes we expect to see the monopole term at its brightest and dimmest, we could properly weight and interpret data at each mode and frequency, enabling us to better compare data points at different points in uv-space and frequency.

So we have established that we can detect the monopole with an interferometer, which is step one. But, as we can see, that sensitivity is faint, especially at the high-frequency end of our science band. That by itself is not wholly problematic – we could just run our observation longer and beat down our sensitivity, assuming we still keep our spacing close enough that our observations don't have to run infinitely long. What is problematic is the strong cross-talk between elements that we know we'll face when we place them that close. We need to make our elements invisible to each other, and we think we can simultaneously enhance our sensitivity to the monopole as well.

In our next set of tests, we include the absorptive baffles around each antenna, as described in previous chapters. Using the absorption profile of the ferrite tiles, as seen in Fig. 4.1, we can see how the monopole sensitivity is changed in the presence of the baffles.

As can be seen in Figures 5.3 and 5.4, the sensitivity of the autocorrelation signal drops off, which is a nice sanity check on this test – less signal from the sky getting picked up by the antenna means less bright visibility on the other end. However, while the spectral shape of the interferometric sensitivity changes, we don't see the same drop in sensitivity in the cross-correlation terms that we do in the auto-correlation. Moreover, as seen in Fig. 5.3, we actually see *increased* sensitivity at the high-frequency end of our science band.

Additionally, we can see in Fig. 5.4 that the baselines no longer completely line up their peaks and nulls in uv-space. This is due to the frequency-dependent nature of the ferrite materials absorptive properties, as seen in Fig. 4.1. If instead the ferrite had no variation in absorption across the science band, we would see a characteristic shape in uv-space that looked much more like Fig. 5.2, where all antenna pairs overlap cleanly in uv-space. This spatial-frequency variance makes it harder for us to calibrate, as we will have to compare the monopole measurements of each baseline only against matching baselines in the array, rather than by matching the measurements at each uv-coordinate in different baseline pairs. It would much better for our calibration and data processing purposes to be able to sample

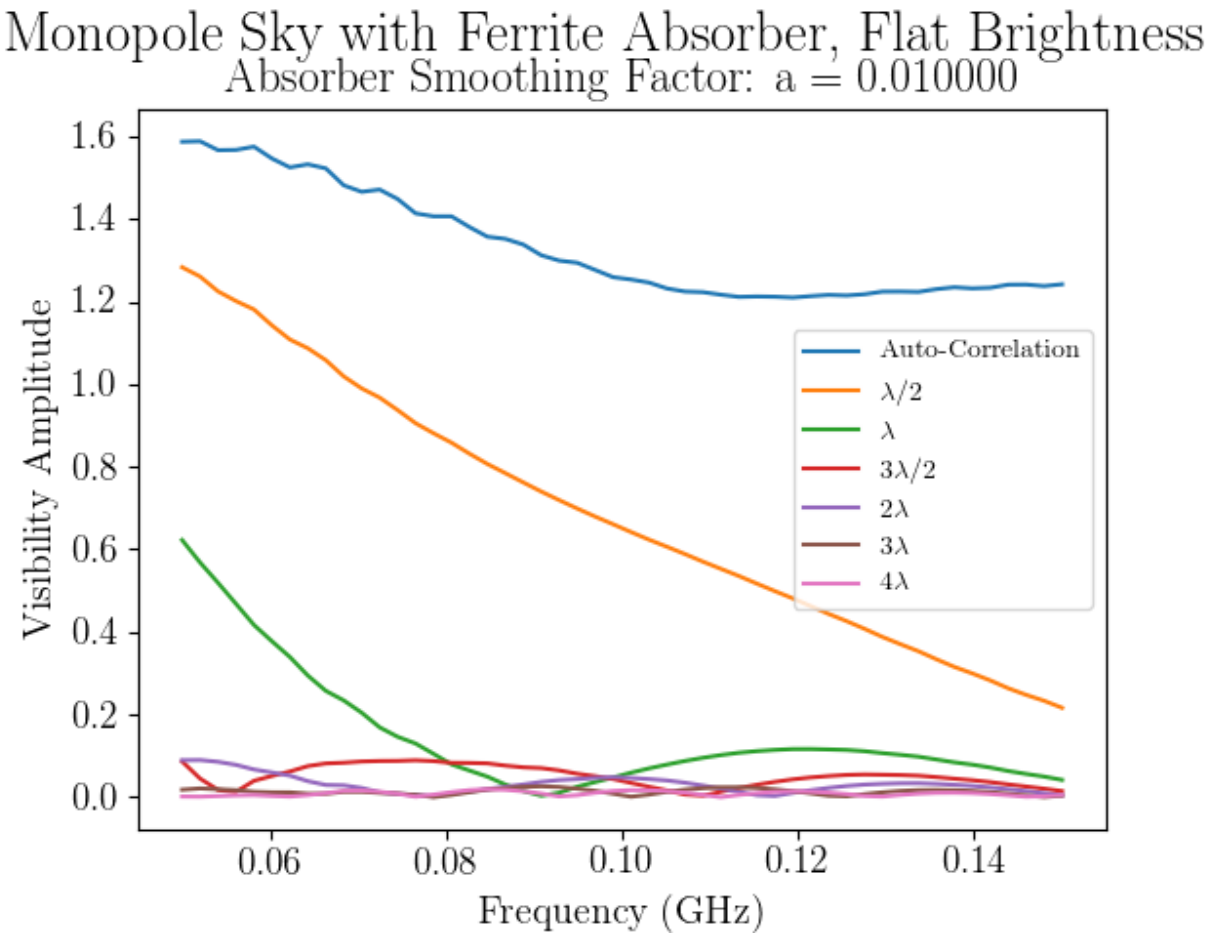

Figure 5.3: Shown here is the absolute value of the visibility of a spectrally flat monopole sky versus frequency, for an array with absorptive baffles constructed from ferrite tiles. In comparison to Fig. 5.1, we see that the reception of the monopole signal has increased at higher frequencies. This indicates that imposing the top-hat windowing function has indeed had the intended effect of pushing the monopole sky into higher-order spatial modes, increasing our array's sensitivity to the global signal.

points of pure non-monopole foreground at multiple frequencies. Therefore, the project would benefit greatly from finding a way to even out the absorptivity of the baffles in frequency space.

5.2 Recovered Global Signal

Finally, we come to the question of whether or not we can accurately interpret our interferometric data in order to actually recover monopole sky, and in doing so observe the 21cm global signal of reionization. More to the point, we want to know if – by knowing this characteristic monopole sensitivity at each frequency – we can combine all of our data from the array, and each baseline separation pairing, and accurately recreate the true global signal.

To do this, we start by performing the exact same calculation described in Eq. (5.1) with a couple of key parameter changes. First off is that our T_{global} is no longer a flat 1.0 K across all frequencies. instead, we import the ARES model of the 21cm reionization global signal, which is similar in its spectral behavior to Fig. 1.1 (Mirocha 2014). We also construct our absorptive baffles out of ferrite tiles, i.e. using an absorption profile matching that of Fig. 4.1. Additionally, we assume that there is a thermal, non-biased temperature to the system, with a flat value across our science band of $T_{sys} = 300$ K. In order to beat down the noise, and in order to give ourselves a fighting chance of a detection, we also integrate for a total of 5 hours of observation over fifty 2 MHz channels, for a total of 100 MHz of observed bandwidth. All in all, this leaves an rms temperature in each frequency bin of about $T_{rms} = 1.6$ mK, which should ensure that our 21cm reionization signal is plenty visible.

Finally, it is worth noting at this point that our array of antennas were arranged in a line, giving us a good set of redundant baselines. We took advantage of these duplicate measurements in this test, in order to give ourselves the best shot we could at (artificially) detecting the global signal.

We can combine all this data – all the baselines and individual integrations over 5 hours and calculated monopole sensitivity coefficients – by using a inverse-variance weighted average to invert our visibility into a brightness temperature.

Specifically, we will be using the characteristic monopole sensitivity coefficients as our weights in an inverse-variance weighting scheme. So, for example, looking at a non-redundant version of our array, for the same frequency bin we would have six different measurements of the visibility, $V(\nu) = [V_{\lambda/2}(\nu), V_{\lambda}(\nu), V_{3\lambda/2}(\nu), V_{2\lambda}(\nu), V_{3\lambda}(\nu), V_{4\lambda}(\nu)]$, where each visibility could be written as:

$$V_i = w_i T_{global} + \sigma \tag{5.2}$$

where w_i is the value of the characteristic monopole sensitivity, T_{global} is the aforementioned global sky temperature, and σ is the expected value of the noise in each measurement. In order to recover an estimated value for the global sky temperature, we must find a way to write T_{global} as a function of the measured visibility, the expected noise, and the weight of the measurement. We can start by first isolating T_{global} from its weight like so:

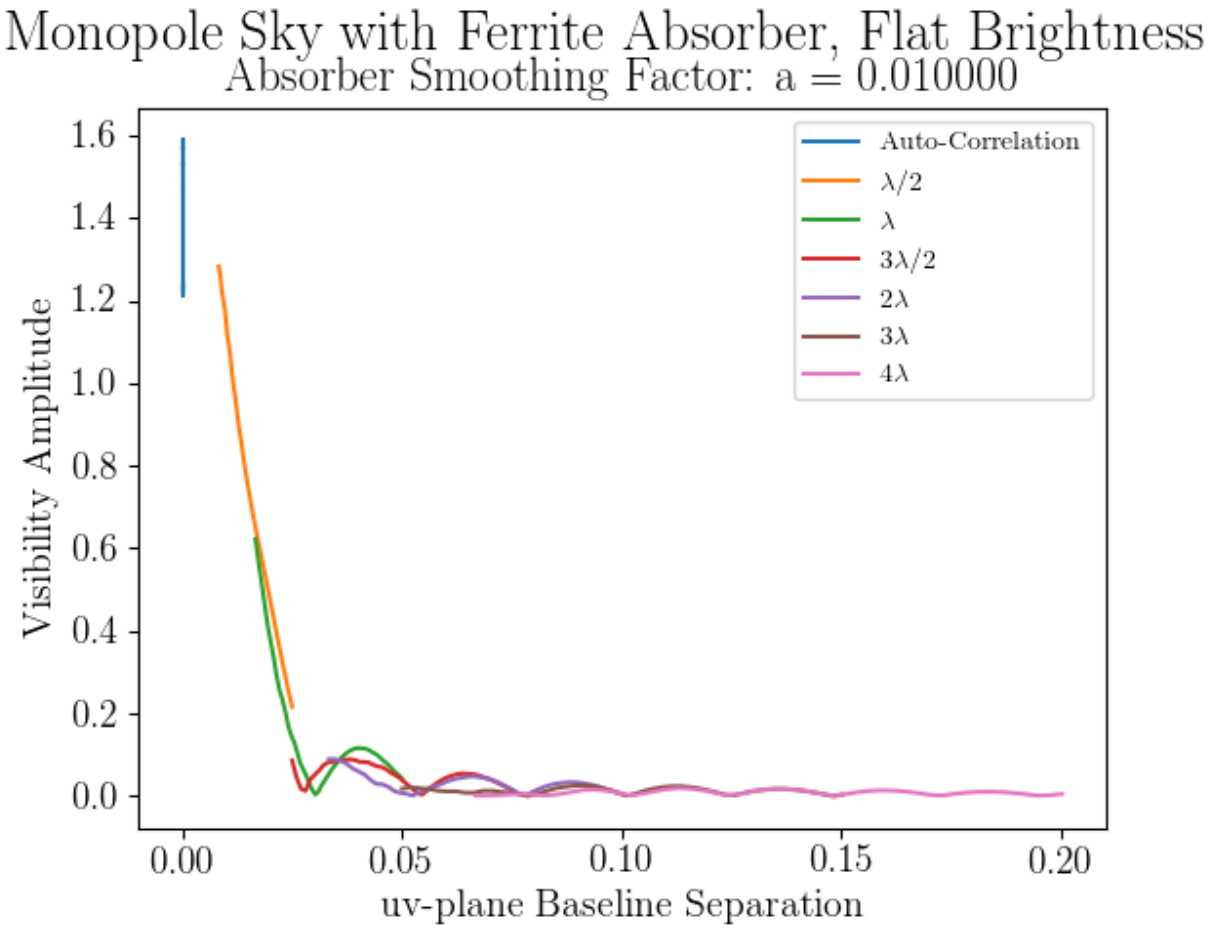

Figure 5.4: Shown here is the absolute value of the visibility of a spectrally flat monopole sky with ferrite absorber walls versus uv-baseline. We can see that, in comparison to Fig. 5.2, the overall shape of the characteristic monopole sensitivity is stretched in *uv*-space, indicating that our imposed top-hat windowing function has had the intended effect of pushing the monopole into higher order (and more sensitive) spatial modes. However, we also see that the sensitivity of the various baseline pairings of the array no longer fall on top of one another. This is due to the frequency-dependent nature of the ferrite as an absorber. Were we to find a way to even out the absorptivity of the baffles in frequency, we would see that the monopole sensitivities would also even out relative to each other, and we would be better able to take advantage of the overlapping samples in *uv*-space.

$$\frac{V_i}{w_i} = T_{global} + \frac{\sigma}{w_i} \tag{5.3}$$

This seems promising, but we must recall that we do have some cases where the sensitivity of our measurement is very low (i.e. $w_i \ll 1$), resulting in a very large value of σ/w_i in your estimate and causing problems. To solve this, we will implement an inverse-variance weighting scheme on our estimation, where the variance of the measurement would be:

$$Var\left(\frac{V_i}{w_i}\right) = \frac{\sigma^2}{w_i^2} \tag{5.4}$$

Weighting our temperature measurement by this factor, we get a recovered temperature estimate of:

$$\hat{T} = \frac{\sum \frac{V_i}{w_i}\frac{\sigma^2}{w_i^2}}{\sum \frac{\sigma^2}{w_i^2}} \tag{5.5}$$

In the case that the expected noise of each measurement is the same (e.g. we would expect that the instrumental noise in the frequency bin would be the same in each measurement), then the noise term actually drops out and the above equation simplifies to become:

$$\hat{T} = \frac{\sum V_i w_i}{\sum w_i^2} \tag{5.6}$$

Finally, the variance on each measurement is given by:

$$Var(\hat{T}) = \frac{\sigma^2}{\sum w_i^2} \sum \frac{1}{w_i} \tag{5.7}$$

As can be seen in Fig. 5.5, this method actually works! Our recovered temperature nearly perfectly recreates the true input signal, with small fluctuations in the brightness temperature only being introduced at high frequencies where the sensitivity is expected to be quite low as compared to the lower frequencies, as seen in Fig. 5.3.

Obviously this case is pretty idealized. Our thermal noise is unbiased and equal across all frequencies. Our sky is nothing but 21cm reionization monopole signal – there is no galactic synchrotron emission nor spatial structure from other sources to account for. Our absorbers have been perfectly understood and characterized.

One thing we know about previous 21cm reionization global signal experiments is that their downfall comes from the fact that they are delicate. Every component of the experiment must be absolutely perfectly understood and calibrated in order to be successful, or their signal will be washed away with the systematics. So far, this has been an order too tall to be filled.

So what if we introduce a nit? What if something wasn't quite perfect with our array? What if, for instance, we didn't quite understand the nature of our absorber walls? In particular, what if we miscalibrated the absorptivity of the walls as a function of frequency?

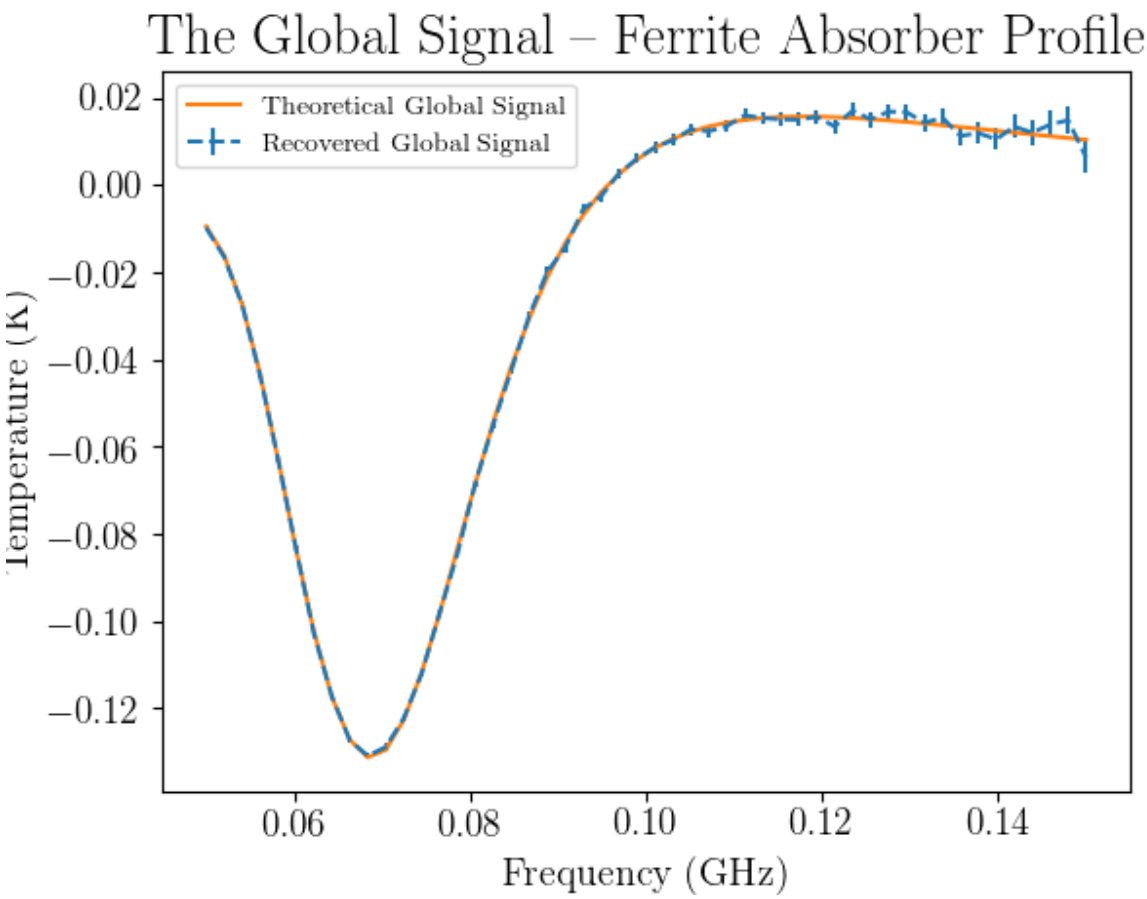

Figure 5.5: Shown here is the recovered reionization global sky temperature, as measured from a maximally redundant seven element east-west array with a total integrated observation time of five hours, a flat system temperature of $T_{sys} = 300$ K, and pure ferrite absorber baffles. As can be seen, this method of observing the global sky temperature works well, with nearly perfect recovery of the true monopole sky at low frequencies (where our array has the highest sensitivities to the monopole mode) and only small fluctuations (on the order of 3 mK) being introduced at the low-sensitivity high-frequency end of our science band. Although this is a highly idealized case, this is a positive result, indicating that our method of weighting observations can accurately recreate the true 21cm reionization global signal.

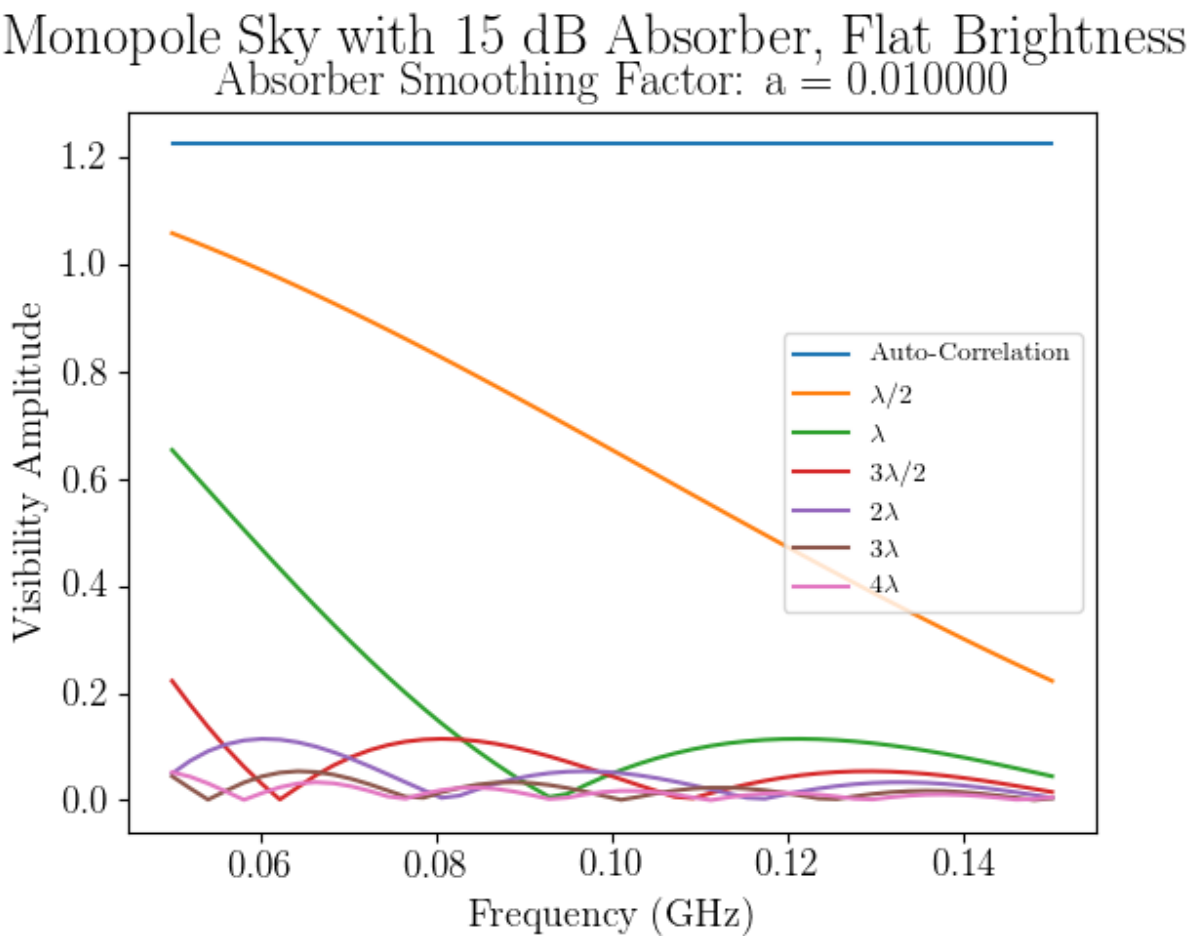

Figure 5.6: Shown here is the absolute value of the visibility of a spectrally flat monopole sky versus frequency, for an array with absorptive baffles constructed from a material with a flat absorptivity of 15 dB across the science band. Overall, this case that the lowest absolute sensitivity to the monopole across the band, but it also has the flattest slope for the drop-off in sensitivity, meaning the whole band has relatively higher sensitivity if an observation is integrated just a little while longer.

In this case, we perform the exact same observation as above. However, where the data was actually collected using ferrite absorptive baffles, the calibration coefficients were calculated assuming a much simpler absorber model: one with a flat 15 dB absorptivity across the whole science band. Instead of having a monopole sensitivity like that seen in Fig. 5.3, it looks like Fig. 5.6. So what happened to our recovered 21cm reionization temperature profile?

Good news! As can be seen in Fig. 5.7, our recovered signal is still largely reflective of the true 21cm reionization global signal. The main difference seen comes at the low frequency

end, where the recovered signal falls just slightly below the true signal up until a frequency of about 80 MHz. In particular, we see that the main absorption feature of the signal is slightly exaggerated, falling approximately 5 mK below the true signal.

This is a promising initial result, indicating that the monopole interferometer may be more robust to minor calibration issues than its single-element counterparts may be. Our recovery isn't perfect in the case of a miscalibration, but it's still *good* – our features are still in the right places, the shapes are still there. No false spectral features have been introduced, suggesting reionization physics that contradicts the reality of the true 21cm reionization global signal. This reassures us that even as we take our system into the backcountry and allow the elements to gently nudge all of our perfect lab calibration to the side, we have constructed a system strong enough to persist in giving us reasonably accurate answers. This result indicates that HYPERION may just have worked.

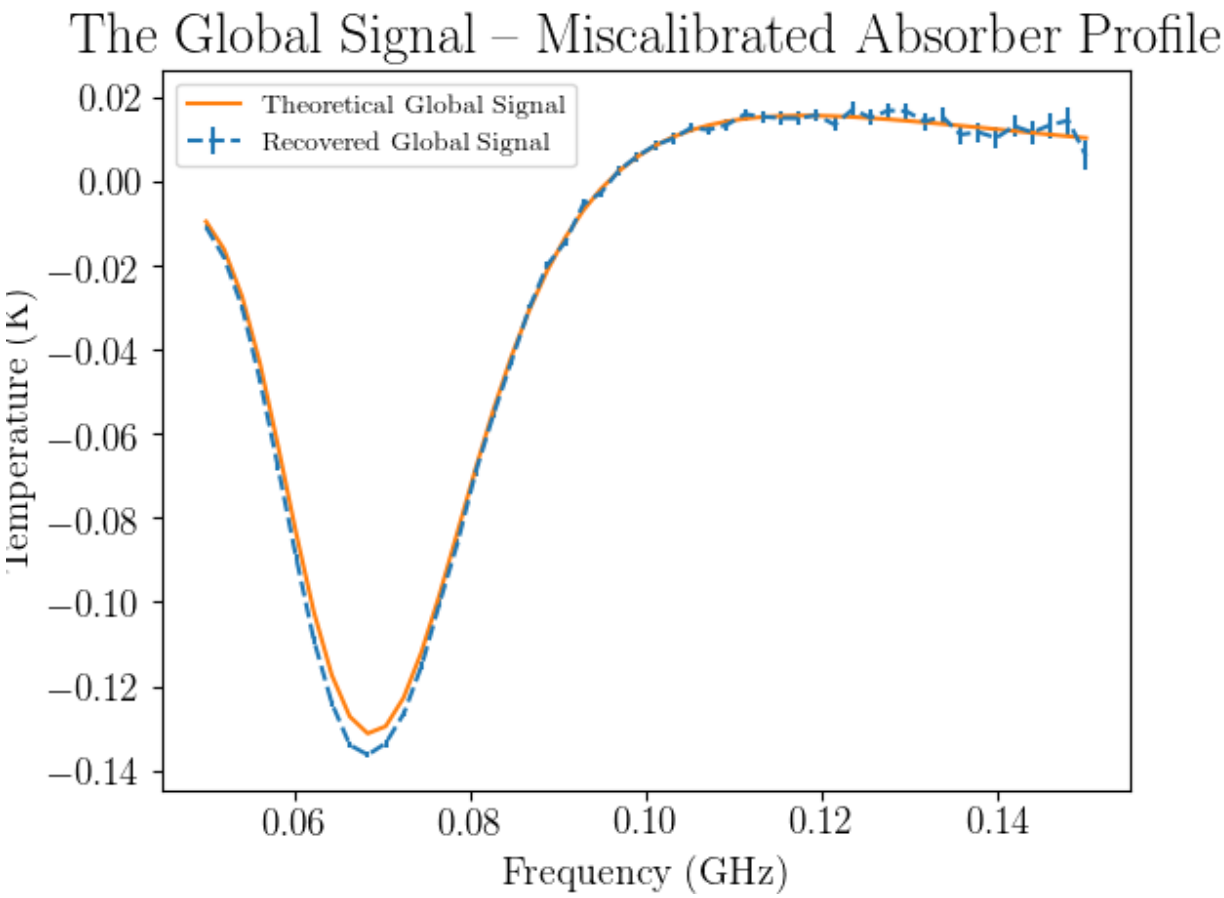

Figure 5.7: Shown here is the recovered reionization global sky temperature, as measured from a maximally redundant seven element east-west array with a total integrated observation time of five hours and a flat system temperature of $T_{sys} = 300$ K. In this case, the data was collected from an array using ferrite absorber baffles, but was calibrated assuming the absorber baffles had a flat absorptivity of 15 dB across the science band. As can be seen, even with this intentional gross miscalibration of the system, we are still able to recreate a fairly accurate portrayal of the true 21cm reionization global signal, with the only major difference being a slight 5 mK exaggeration of the depth of the absorption feature. This indicates that our weighting method is robust to an imperfect calibration of the performance of the absorptive baffles – a promising result for the feasibility of the project.

Chapter 6

Conclusion

As we have shown, the ideas behind HYPERION are sound. We can manipulate our sensitivity to the global signal by imposing a step function onto the beam of our antennas – thereby converting the monopole mode into a series of higher order modes with known scale coefficients. We can create this step function both by building HYPERION on the Earth and using the pre-existing horizon to our advantage, and by artificially raising that horizon by building absorptive walls around each antenna. Through in-lab testing, we have found that the most promising absorptive material at our low-frequency ranges is ferrite, though we are also interested in the idea of a resistive mesh, either on its own or layered with the ferrite, depending on its performance. Once we know about the final overall performance of an absorber across our science band, we can simulate a given array design's sensitivity to the monopole sky, and thereby generate the scale coefficients for each antenna pairing in the array. We can use these scale coefficients to the calibrate and process the observational data, recovering the monopole sky and finally getting a glimpse of the global signal.

These results are quite promising, particularly because, as seen in Fig. 5.7, this data processing method is robust against at least some types of miscalibration. We were able to completely mismatch the true and simulated absorber profiles, and ended up recovering a global signal that was only approximately 5% different from the true input signal. This indicates that, should HYPERION ever be constructed, those operating it need not worry about constantly monitoring the state of the absorber baffles to get a perfectly accurate measure of their absorptivity for each measurement made – so long as we take care in our initial measurements of the absorber baffles, we can be confident that they will remain good enough to provide us excellent results in our observations.

Now that we know that these measurements are feasible, and possibly more robust to systemic error than our experimental predecessors, we must now continue to seek a better understanding of our instrumental design and how to optimize it in the face of real observational adversity. So far, we have taken the very optimistic view in our simulations that the sky is purely monopole, that there are no higher order modes in our signal. In reality, we know that the sky at these frequencies is full of galactic structure and extragalactic point sources. We simply don't know how well this method of data analysis will work when we

have a realistically spatially-polluted sky.

The next step to prove the merit of a monopole interferometer would be to input a complex sky into the model and see how it behaves. Using accurate global sky models alongside our theoretical reionization signal, we can perform the same process described in Section 5.2 and assess our ability to recover the reionization global sky, and develop new tools as necessary.

We must also further investigate the realities of the absorbers and how best to construct them. To start, we may first assess the viability of the resistive mesh concept, testing its absorption across our frequency band and comparing it to that of the ferrite tiles. Next, we must begin to explore the full electromagnetic system of our antenna-absorber pairs. How does diffraction affect our absorber spatial profile? Is there coupling between the absorber and the antenna? If so, how does that change our results?

The answers to these questions will determine the long-term viability of this method. At present, all we know is that the idea behind a monopole interferometer is far less far-fetched than it may have originally seemed. With proper calibration and experimental design, it very well could serve a key place in the search for understanding of the epoch of reionization.

Appendix A

The Flat-Sky Approximation and Its Limitations

In Eq. (2.5), we made one implicit assumption – that we are working in only two dimensions. This, of course, is not true.

In reality, if one is hoping to utilize the nice Fourier nature of the brightness and visibility planes, the van Cittert-Zernicke theorem should be written in terms of *(u,v,w)* coordinates, rather than just *(u,v)*. The full (idealized) measurement equation can thus be written as:

$$V(u,v,w) = \iint I(l,m) e^{-2\pi i(ul+vm+w\sqrt{1-l^2-m^2})} dl dm \tag{A.1}$$

The next step is to assume that l and m are small, such that $\sqrt{1-l^2-m^2} \approx 1$, allowing the $e^{-2\pi i w}$ term to be removed from the integral by applying the proper phasing to the measured visibility and the measurement equation to be simplified to a 2D Fourier transform sampled in the uv-plane. This procedure is called the *flat-sky approximation*.

This approximation works well for many applications in astronomy, particularly in the observation of point sources or small extended sources in the sky (up to about $\pm 10°$ or so, where $l \equiv \sin\theta \approx \theta$). However, as the observed area in the sky gets larger, it becomes impossible to apply an absolutely correct phasor to the 2D integral, and the w-term instead introduces a spatially varying departure from the 2D Fourier transform the further from the phase center you are.

So, obviously, in the case where you're trying to use an interferometer to observe a global phenomenon (such as the reionization global signal), the flat sky approximation simply won't do. In the case that one is attempting to perform sky imaging, then care must be taken to navigate the pitfalls of the flat-sky approximation, including the use of clunky or expensive algorithms such as W-projection. In our case, we are not trying to image the sky at all, rather we're just attempting to understand the distribution of power in the visibility domain. We can therefore avoid the (u,v) to (l,m) confusion entirely and calculate our visibilities directly based on our knowledge of the source direction $\mathbf{s}$ and the baseline separation $\mathbf{b}$.

Bibliography

Bowman, J. D., Rogers, A. E. E., Monsalve, R. A., Mozdzen, T. J., & Mahesh, N. 2018, Nature, 555

Burns, J. O. e. a. 2012, Advances in Space Research, 49

DeBoer, D. R. e. a. 2017, Publications of the Astronomical Society of the Pacific, 129

Essinger-Hileman, T., Halverson, N., Hanany, S., et al. 2016, CMB S-4: Telescope Design Considerations, Tech. rep.

Fixsen, D. J. 2009, The Astrophysical Journal, 707, 916

Furlanetto, S. R., Oh, S. P., & Briggs, F. H. 2006, Physics Report, 433

Haslam, C. G. T., Salter, C. J., Stoffel, H., & Wilson, W. E. 1982, Astronomy and Astrophysics, 47

Kundert, K. 2016, The Relationship Between System Temperature and Sky Beam Coverage, Memo 1, HYPERION

Mahesh, N., Subrahmanyan, R., Udaya Shankar, N., & Raghunathan, A. 2015, IEEE Transactions on Antennas and Propagation, 63

Mirocha, J. 2014, Monthly Notices of the Royal Astronomical Society

Monsalve, R. A., Rogers, A. E. E., Bowman, J. D., & Mozdzen, T. J. 2017, The Astrophysical Journal, 847

Patra, N., Subrahmanyan, R., Raghunathan, A., & Shankar, N. U. 2013, Experimental Astronomy, 36

Penzias, A. A., & Wilson, R. W. 1965, The Astrophysical Journal, 142, 419

Presley, M. E., Liu, A., & Parsons, A. R. 2015, The Astrophysical Journal, 809

Pritchard, J. R., & Loeb, A. 2010, Physical Review D, 82

—. 2012, Reports on Progress in Physics, 75

Rogers, A. E. E., & Bowman, J. D. 2008, The Astronomical Journal, 136

Rottgering, H. J. A. e. a. 2006, in Proceedings of the Conference on Cosmology, Galaxy Formation, and Astroparticle Physics on the Pathway to the SKA (Oxford)

Venumadhav, T., Chang, T.-C., Doré, O., & Hirata, C. 2016, The Astrophysical Journal, 826

Voytek, T. C., Natarajan, A., García, J. M. J., Peterson, J. B., & López-Cruz, O. 2014, The Astrophysical Journal Letters, 782

Wright, E. L. e. a. 1992, The Astrophysical Journal Letters, 396, L13

Zaroubi, S. 2012, in The First Galaxies, – Theoretical Predictions and Observational Clues, ed. T. Wiklind, B. Mobasher, & V. Bromm (Springer), 45–101